Supporting Information

Chromium-leaching induced electronic structure modulation in CoOOH for improved alcohol oxidation reactions

Vishesh Kumar[a] Vijay Patel[a] and Arindam Indra*[a]

[a]Department of Chemistry, Indian Institute of Technology (BHU), Varanasi, UP-221005, India.

E- mail: arindam.chy@iitbhu.ac.in

Chemicals

Potassium hexacyanocobaltate(III) $K_3[Co(CN)_6]$, tri-sodium citrate dihydrate ($C_6H_5Na_3O_7 \cdot 2H_2O$), cobalt(II) acetate tetrahydrate $Co(CH_3COO)_2.4H_2O$, $CDCl_3$ and DMSO-d_6 were purchased from Sigma-Aldrich. Chromium(III) nitrate nonahydrate [$Cr(NO_3)_3.9H_2O$], potassium hydroxide, ethyl acetate, ethanol, and hexane were purchased from Merck. All benzyl alcohol derivatives were purchased from either Avra Synthesis Pvt Ltd., India, Sigma Aldrich, or Tokyo Chemical Industry Co., Ltd., Japan.

Instrument

The powder X-ray diffraction patterns (PXRD) were recorded in the 2-theta range of 5°-80°. The PXRD was recorded on a Rigaku D/MAX RINT-2000 X-ray diffractometer. The Cu-Kα (λ = 1.5418Å) radiation was utilised for the PXRD measurement.

X-ray photoelectron spectroscopy (XPS) was carried out using VG/VG ESCA LAB 220i X-ray photoelectron spectrometer to determine the synthesised catalysts' chemical nature, oxidation state, and surface structure. The XPS data were deconvoluted and analysed using Origin 8.5 software.

Scanning electron microscopy (SEM) using a field emission scanning electron microscope, EVO-Scanning electron microscope MA15/18, was utilised to investigate the morphology and surface characteristics. The energy dispersive X-ray (EDX) analysis was carried Team Pegasus Integrated EDS-EBSD.

Raman spectra were recorded in an STR-300 spectrometer (AIRIX Corp.) with a 532 nm excitation source.

Fourier-transform infrared (FT-IR) spectra of catalysts were recorded using a Thermo Scientific Nicolet iS5 FTIR spectrometer.

Transmission electron microscopy (TEM) was performed using a Tecnai G2 20 TWIN transmission electron microscope.

^{1}H-NMR and ^{13}C-NMR spectra were obtained using the AVH D 500 AVANCE III HD 500 MHz One Bay NMR Spectrometer from Bruker Bio Spin International and Advance Neo 600 MHz Bruker India Scientific. The chemical shifts and coupling constants were reported in ppm. The abbreviations used are as follows: "s" for singlet, "bs" for broad singlet, "d" for doublet, "t" for triplet, and "m" for multiplet. Residual solvent signals ($CDCl_3$: δ_H = 7.28-7.29 ppm and δ_C = 77.01-77.16 ppm) and (DMSO-d_6: δ_H = 2.5 ppm and δ_C = 39.52-40.00 ppm) were used as the references for ^{1}H and ^{13}C NMR spectra, respectively.

Experimental

Synthesis of CoCo-PBA

0.15 g $Co(CH_3COO)_2 \cdot 4H_2O$ and 0.26 g $C_6H_5Na_3O_7 \cdot 2H_2O$ were dissolved in 20 mL distilled water to form solution A. 0.13 g $K_3[Co(CN)_6]$ was dissolved in 20 mL distilled water to form solution B. Subsequently, solution B was added into solution A under magnetic stirring and then the mixture was aged at room temperature for 24 h. Finally, the precipitate of CoCo-PBA was centrifuged out and washed with distilled water and ethanol, followed by drying at 60 °C overnight in a hot air oven.[1]

Synthesis of CrCo-PBA

0.39 g $Cr(NO_3)_3.9H_2O$ and 0.88 g of $C_6H_5Na_3O_7 \cdot 2H_2O$ were dissolved in 20 mL distilled water to form solution A. The pH of the solution was increased to 8 with the addition of 10% NH_3 solution. Next, 0.53 g of $K_3[Co(CN)_6]$ was dissolved in 20 mL distilled water to form solution B. Solution B was added to solution A under stirring, and then the mixture was aged at room temperature for 24 h. Finally, the precipitate of CrCo-PBA was centrifuged out and washed with distilled water and ethanol, followed by drying at 60 °C overnight in a hot air oven.

Activation of nickel foam (NF)

NF pieces (1 × 2 cm) were washed with acetone and rinsed several times with distilled water. The cleaned NF was then sonicated in 1.0 M HCl for 10 min, followed by additional rinsing with distilled water, and dried in a hot air oven at 50 °C for 12 h.

Electrode preparation

3 mg catalyst was dispersed in 500 μL ethanol and 20 μL Nafion solution (0.05 wt.%), followed by the sonication for 15 min. The resulting suspension was drop-cast onto a nickel foam electrode (1×1 cm^2) to ensure uniform coating and subsequently dried at 60 °C for 3 h in a hot-air oven. The final catalyst loading was 3.0 mg cm^{-2}.

Electrochemical measurements

Electrochemical OER measurements were conducted in a single-compartment three-electrode cell using 1.0 M aqueous KOH as the electrolyte, while benzyl alcohol (BA) oxidation was performed in 1.0 M KOH containing 2 mmol BA. The catalyst-coated nickel foam served as the working electrode, with a Pt wire as the counter electrode and Hg/HgO electrode as the reference. Cyclic voltammetry (CV) and linear sweep voltammetry (LSV) were recorded with 25% i*R* compensation, and all potentials were converted to the reversible hydrogen electrode (RHE) scale using the equation:

$$\mathbf{E_{(RHE)} = E_{(Hg/HgO)} + 0.098 + 0.059pH}$$

Tafel plots were determined by potentiostatic measurements at the potentials where current density was reached up to at least 10 mA cm^{-2}. The Tafel slope was calculated using the Tafel equation:[2]

$$\mathbf{\eta = b \log j + a}$$

where η denotes the overpotential (V), j is the current density (mA cm^{-2}), and b is the Tafel slope (mV dec^{-1}).

Electrochemical impedance spectroscopic (EIS) measurements were recorded in the frequency range from 0.001 to 100,000 Hz with an amplitude of 10 mV at a potential of 1.5 V *vs.* RHE. The charge transfer resistance (R_{ct}) was calculated from the diameter of the semicircle in the Nyquist plots.

The electrochemically active surface area (ECSA) of the catalysts was evaluated by determining the double-layer capacitance (C_{dl}). For C_{dl} measurements, CV was carried out at a potential range (0.92 to 1.02 V *vs.* RHE) where no apparent faradaic process occurred. The ECSA of the catalysts was determined by the equation ECSA

= C_{dl} /*C*s, where Cs (20 mF cm^{-2}) represents the specific capacitance of the material for a standard with 1 cm^2 of the real surface area under identical electrolyte conditions.

General procedure

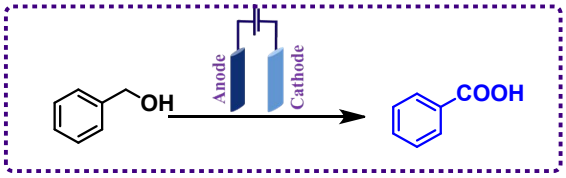

Reaction conditions for benzyl alcohol oxidation reactions (BOR): The electrocatalytic BOR was performed in a three-electrode configuration using catalyst@NF as the working electrode, Pt as the counter electrode, and Hg/HgO as the reference electrode. The reaction was carried out in a 20 mL electrochemical cell under chronoamperometric (CA) conditions at a constant potential of 1.45 V *vs.* RHE for 2.5 h, until otherwise mentioned. Since the highest conversion and faradaic efficiency (FE) were achieved at 1.45 V *vs.* RHE, BA oxidation was further evaluated with other catalysts under identical reaction conditions.

Calculation of product selectivity and Faradaic efficiency

The selectivity and FE were calculated using the equation below:

$$\text{Selectivity (\%)} = \frac{\text{Mole of the target product}}{\text{Mole of all the detected products}} \times 100\ \%$$

$$\text{FE (\%)} = \frac{\text{Mole of produced product}}{\text{Total charge passed}/(n \times 96485)} \times 100\ \%$$

Where, F represents the Faraday constant (96,485 C mol^{-1}), and n denotes the number of electrons involved in the oxidation reaction (4 e^-). After 2.5 h of electrolysis, the potentiostat recorded a total charge of 775.69 C during BOR. Based on the experimental values, a final FE of 99 % was obtained after 2.5 h of reaction.

Separation of benzoic acid

During the reaction, the generated benzoic acid initially exists as potassium benzoate (Ph–COOK) in the KOH electrolyte. Upon completion, the reaction mixture was neutralised with 1.0 M HCl to convert Ph–COOK into Ph–COOH. The resulting mixture was kept in a fridge for the crystallisation of benzoic acid, the solid was filtered and purified through multiple recrystallisations in hot water to eliminate KCl impurities. For recrystallisation, the crude crystals were dissolved in hot water (80 °C) and allowed to cool slowly, and high-purity benzoic acid crystals were collected by filtration. The product yield was determined using the isolated yield method, and the formation of benzoic acid was verified by ^{1}H and ^{13}C NMR spectroscopy, confirming nearly 100 % selectivity.

Measurement of the produced hydrogen

Hydrogen generation during both OER and BOR was measured in an H-type cell using the water displacement method under a two-electrode system. Chronoamperometric tests were conducted at 1.45 V *vs.* RHE for 30 minutes, after which the collected volume of hydrogen (mL) was converted to mmol for quantitative analysis.

Figures

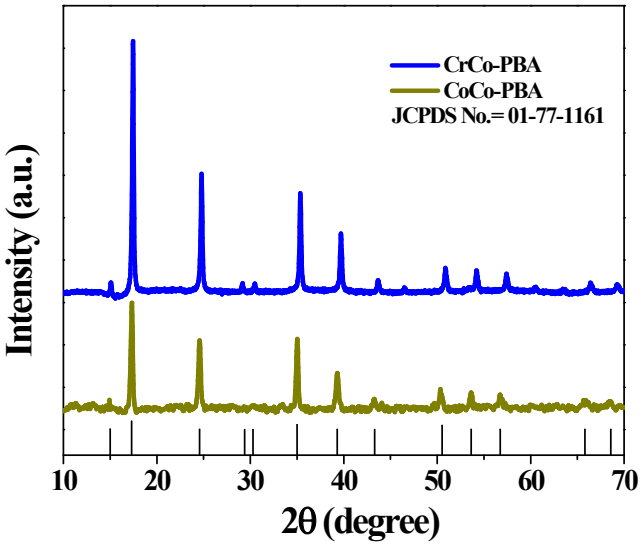

Figure S1. PXRD pattern of CoCo-PBA and CrCo-PBA, matched with JCPDS no. 01-77-1161.[2]

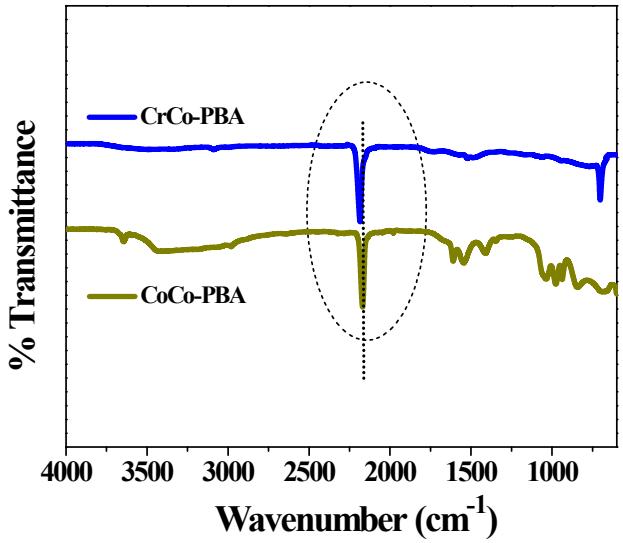

Figure S2. IR spectra of CoCo-PBA and CrCo-PBA revealed characteristic peaks corresponding to the stretching vibrations of the bridging –CN group.

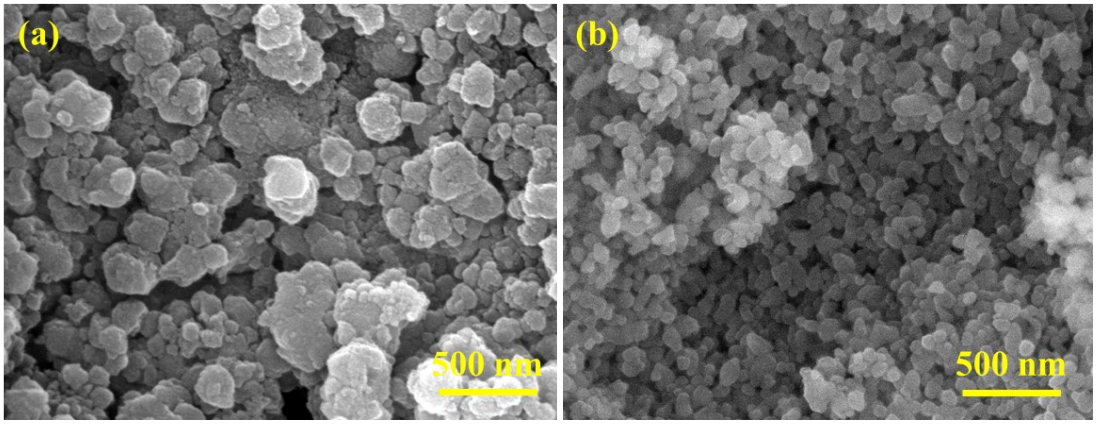

Figure S3. SEM image of (a) CrCo-PBA and (b) CoCo-PBA.

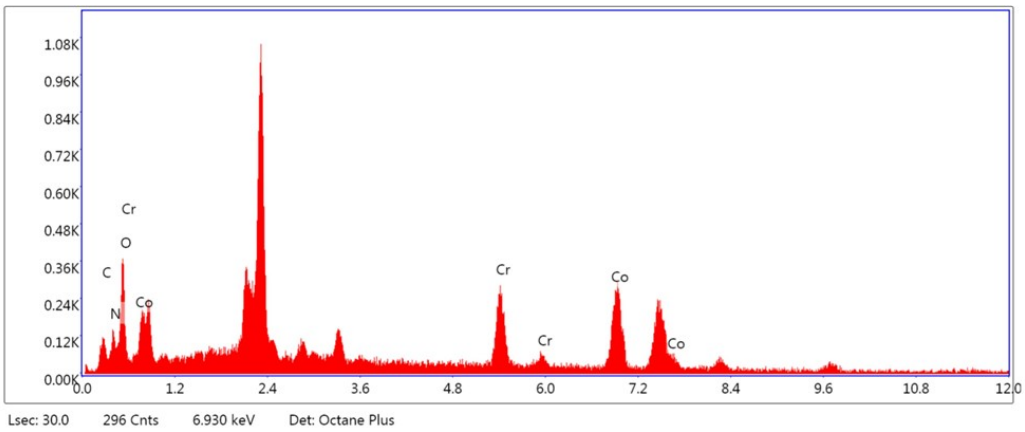

Figure S4. Energy dispersive X-ray (EDX) spectrum of CrCo-PBA showing the presence of elements Cr, Co, N, and C**.**

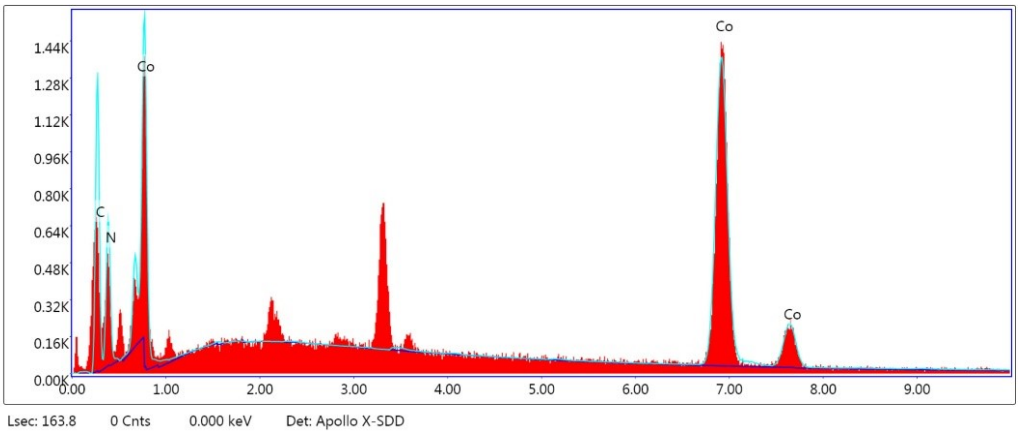

Figure S5. Energy dispersive X-ray (EDX) spectrum of CoCo-PBA showing the presence of the elements Co, C, and N**.**

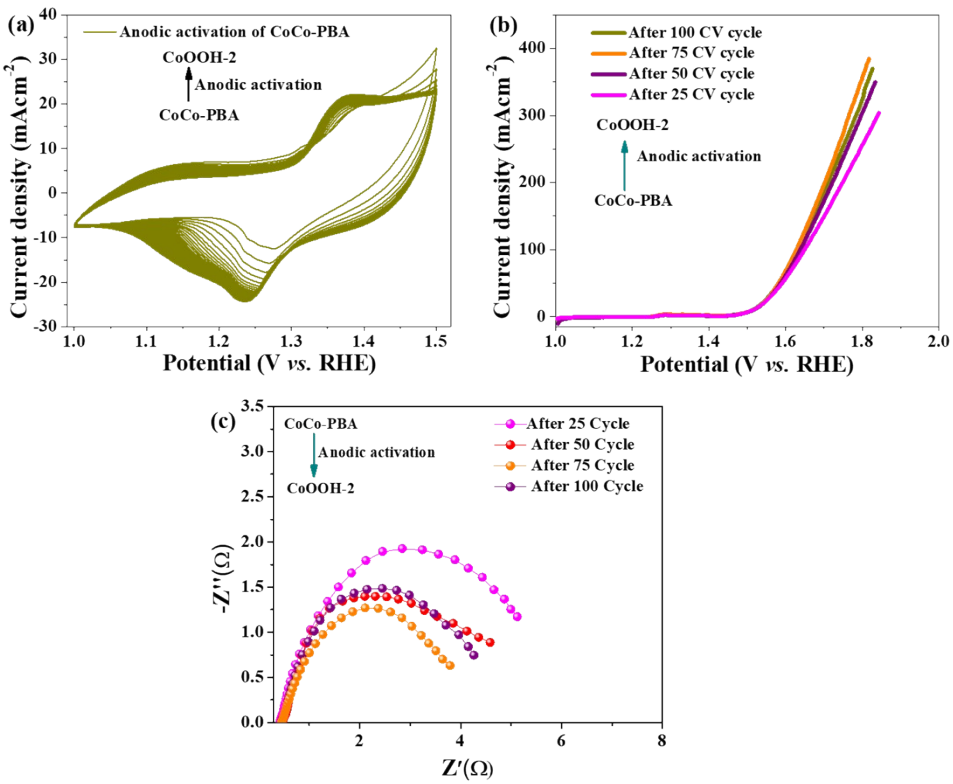

Figure S6. (a) CV activation of CoCo-PBA to form the active phase CoOOH-2. (b) Corresponding LSV profiles recorded at various activation cycles. (c) EIS spectra obtained at different activation cycles.

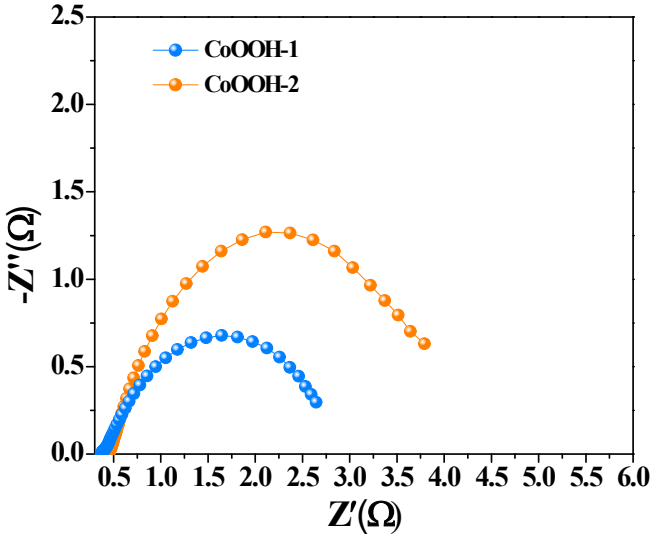

Figure S7. EIS plots of CoOOH-1 and CoOOH-2.

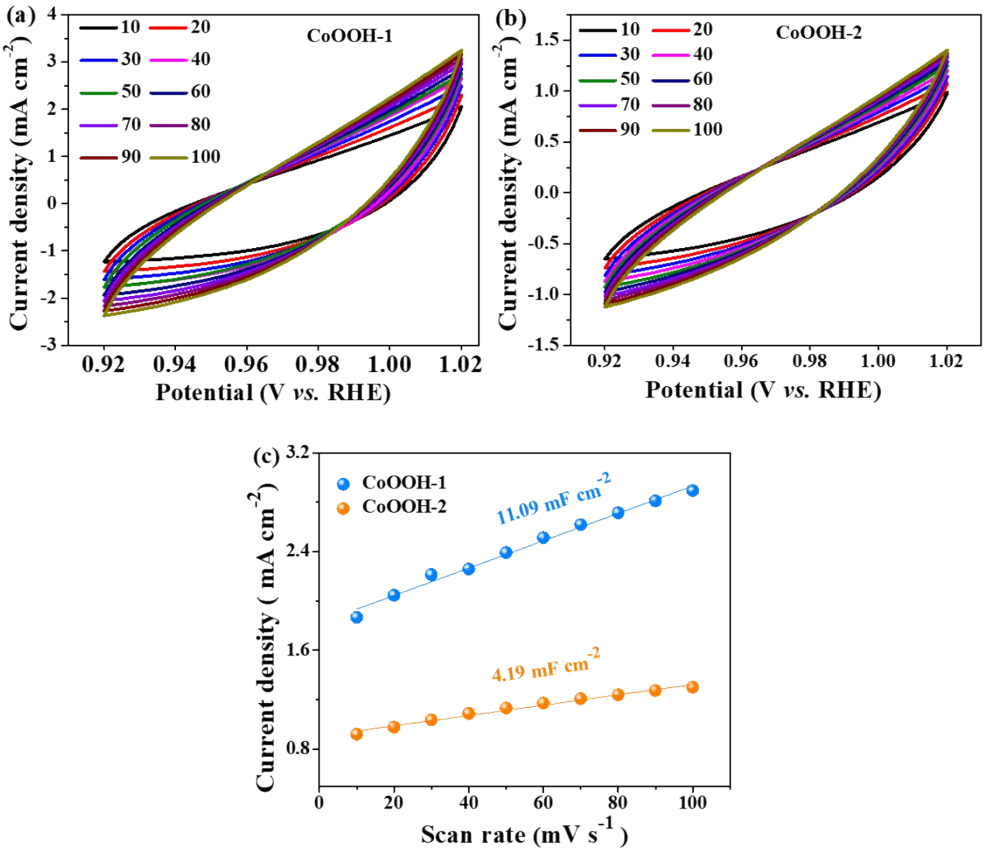

Figure S8. The electrochemical capacitance current of all (a) CoOOH-1 and (b) CoOOH-2 was analysed within the non-Faradaic potential range from 0.92 V to 1.02 V *vs.* RHE. (c) The determination of double-layer capacitance (C_{dl}) involved plotting the (difference in current density)/2 against the scan rate.

The specific capacitance of 1 cm^2 flat surface area is in the range of 20-60 μF cm^{-2}, which can be averaged to 40 μF cm^{-2}. The C_{dl} value was converted to the electrochemical surface area (ECSA) using the equation:

ECSA = (C_{dl} of catalyst in mF cm^{-2}/0.04 mF cm^{-2}) cm^2.

ECSA of **CoOOH-1** = (11.09 mF cm^{-2}/0.04 mF cm^{-2}) cm^2 = **277.25 cm^2**

ECSA of **CoOOH-2** = (4.19 mF cm^{-2}/0.04 mF cm^{-2}) cm^2 = **104.75 cm^2**

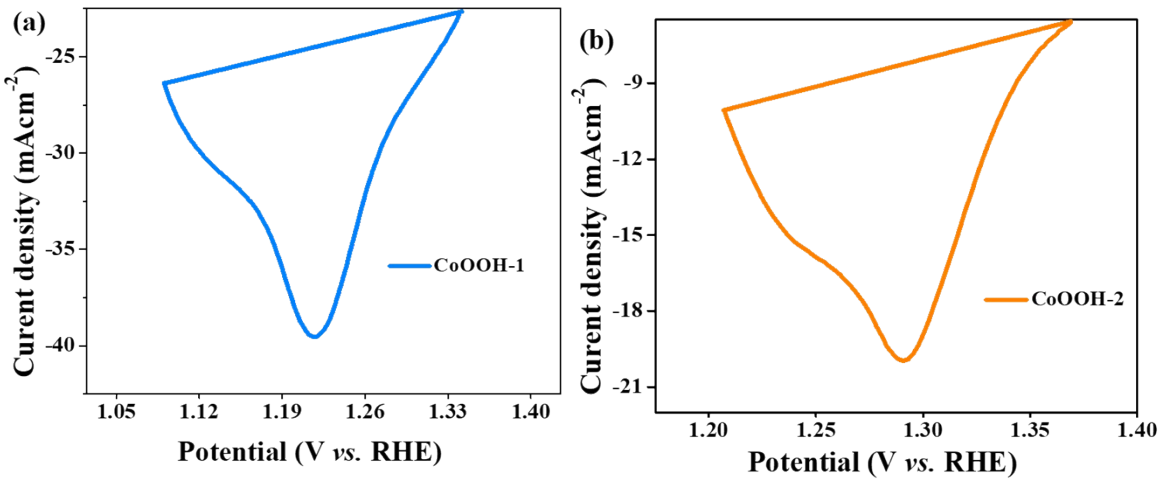

Figure S9. The reduction peak area of the catalysts CoOOH-1 and CoOOH-2 was used to determine the number of active sites.

Equation S1: Determination of surface-active sites using area integration of reduction peaks.

For CoOOH-1

The calculated total area associated with the reduction peak = 1.73×10^{-3} V A

Hence, the associated charge is = 1.73×10^{-3} V A / 0.005 V s^{-1}

= 346×10^{-3} A s

= 346×10^{-3} C

Now, the number of electron transferred is = 346×10^{-3} C / 1.602×10^{-19} C

= 215.98×10^{16}

Since the reduction of Cr^{3+} to Co^{2+} is a single-electron transfer reaction, the number of electrons calculated above is the same as the number of surface-active sites.

Hence, the surface-active site that participated in OER is = **215.98×10^{16}**

For CoOOH-2

The calculated area associated with the reduction peak = 0.92×10^{-3} V A

Hence, the associated charge is = 0.92×10^{-3} V A / 0.005 V s^{-1}

= 184×10^{-3} A s

= 184×10^{-3} C

Now, the number of electron transferred is = 184×10^{-3} C / 1.602×10^{-19} C

= 115×10^{16}

Since the reduction of Co^{3+} to Co^{2+} is a single-electron transfer reaction, the number of electrons calculated above is the same as the number of surface-active sites.

Hence, the surface-active site that participated in OER is = **114.84×10^{16}**

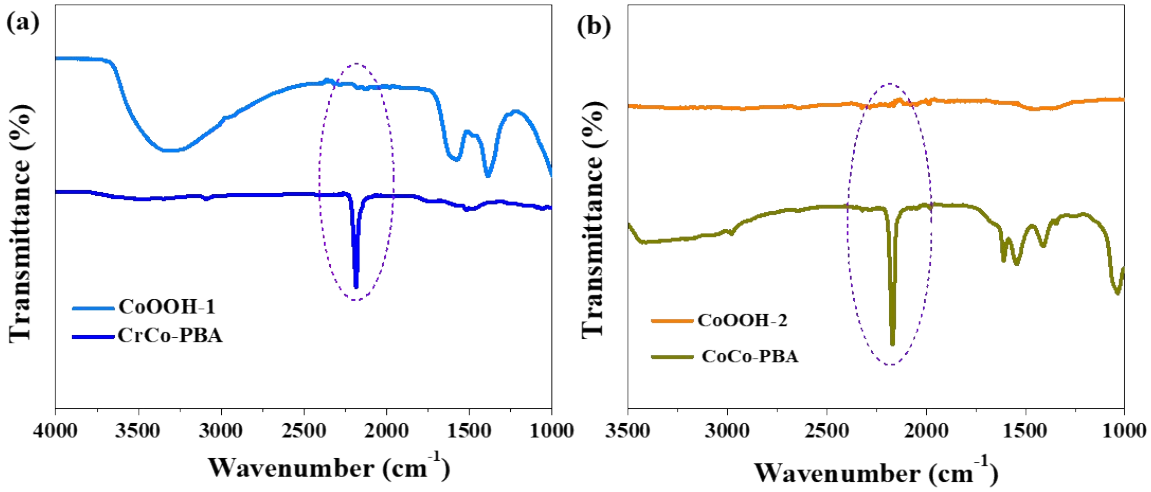

Figure S10. (a) IR spectra of CoOOH-1, attained by the anodic activation of CrCo-PBA. (b) IR spectra of CoOOH-2, attained by the anodic activation of CoCo-PBA. The disappearance of bridging –CN peak confirms the complete conversion of PBAs into active catalysts.

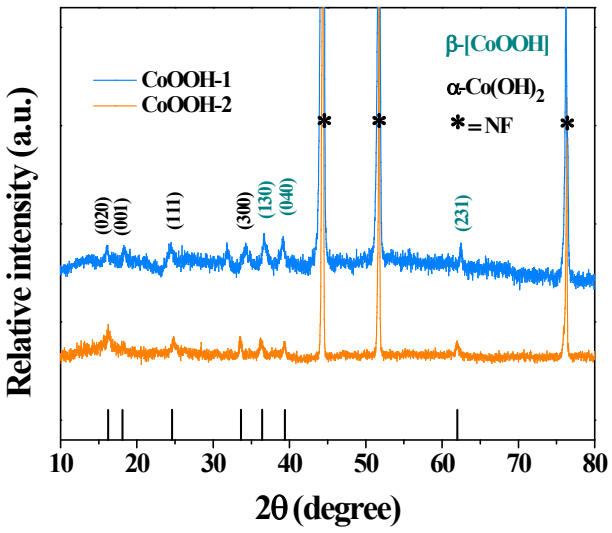

Figure S11. PXRD of anodically activated PBAs (CoOOH-1@NF and CoOOH-2@NF) shows peaks indexed to mixed phases of β-Co(O)OH (JCPDF 26-0480) and α-$Co(OH)_2$ (JCPDF 48-0083).[2]

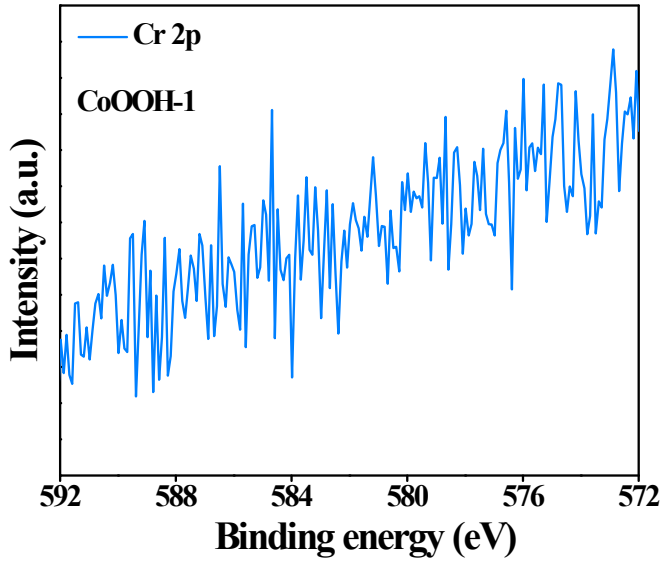

Figure S12. Cr 2p XPS of CoOOH-1. The Cr 2p XPS confirmed that the Cr was leached out during the anodic activation process.

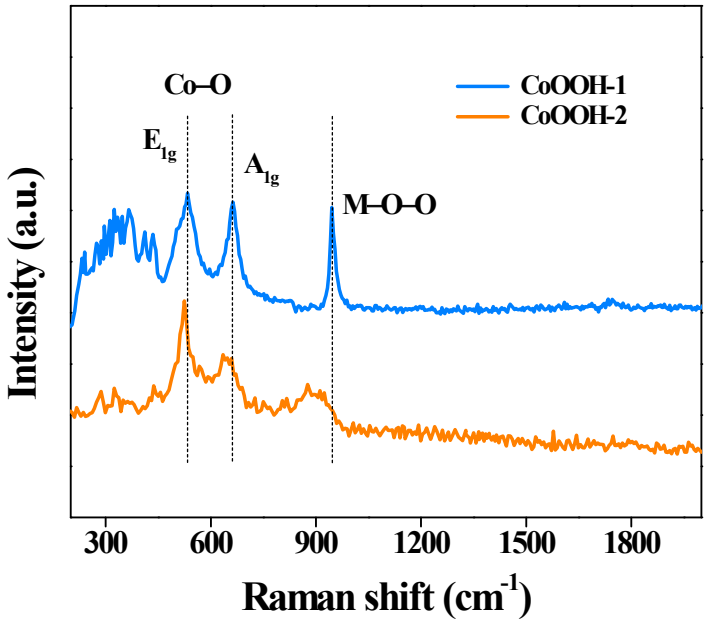

Figure S13. Raman spectra of CoOOH-1 and CoOOH-2.

Table S1: Comparison of CoOOH-1 and CoOOH-2 catalysts, highlighting the electronic structure modulation.

Catalyst	Co $2p_{3/2}$ binding energy (from XPS)	Co^{3+}/Co^{2+} ratio (from XPS)	Raman shift of E_g band	Raman shift of A_{1g} band
CoOOH-1	780.66 eV	1.01	533 cm^{-1}	662 cm^{-1}
CoOOH-2	780.10 eV	0.36	524 cm^{-1}	644 cm^{-1}

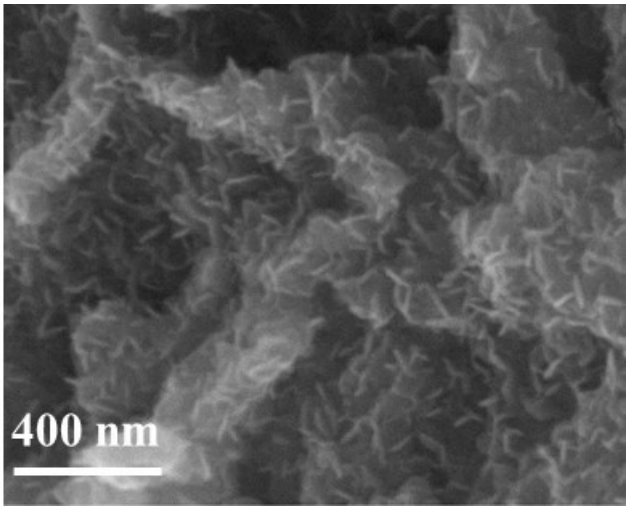

Figure S14. SEM image of CoOOH-2.

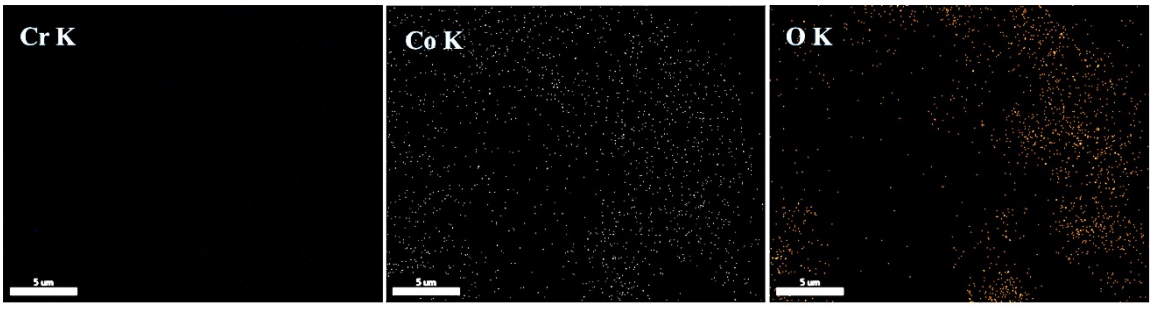

Figure S15. Elemental mapping of CoOOH-1 shows the uniform distribution of Co and O, while Cr is largely leached out during anodic activation.

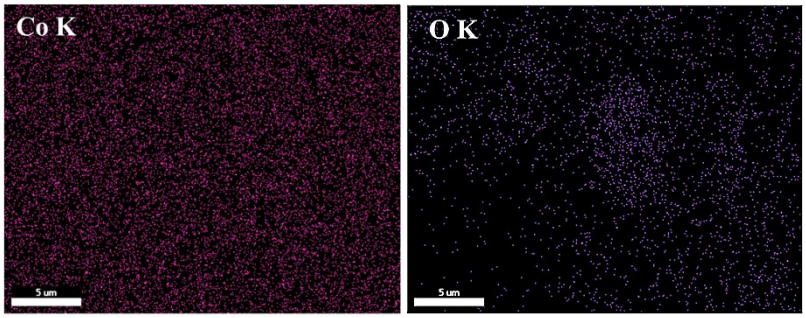

Figure S16. Elemental mapping of CoOOH-2 shows uniform distribution of Co and O.

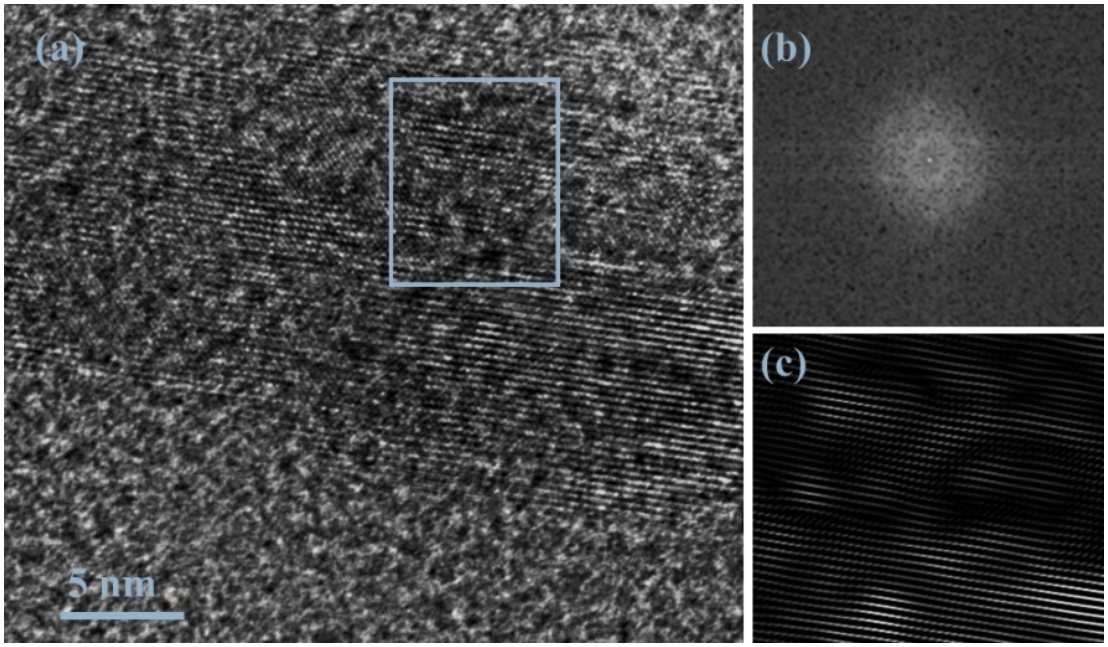

Figure S17. (a) HR-TEM, (b) FFT, and (c) inverse FFT of CoOOH-1.

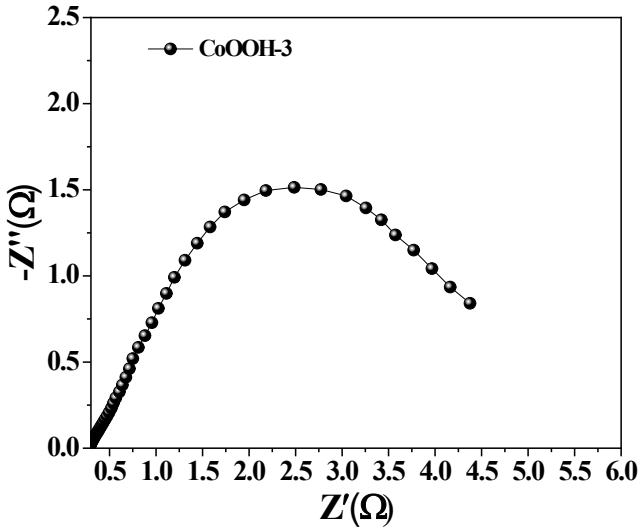

Figure S18. EIS of CoOOH-3.

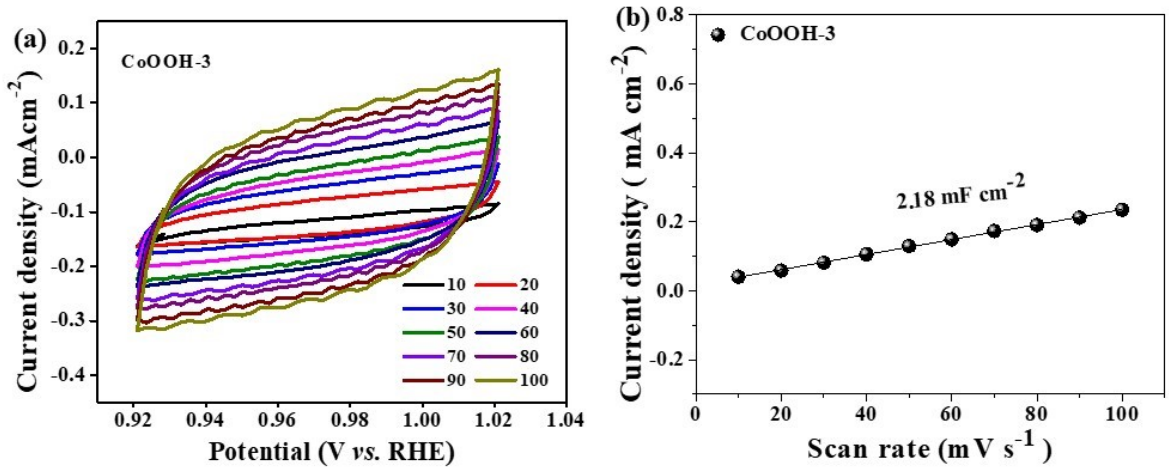

Figure S19. (a) The electrochemical capacitance current of CoOOH-3 in the non-Faradaic potential range from 0.92 V to 1.02 V *vs.* RHE. (b) Double-layer capacitance (C_{dl}) for CoOOH-3.

ECSA of **CoOOH-3** = (2.18 mF cm^{-2}/0.04 mF cm^{-2}) cm^2 = **54.50 cm^2.**

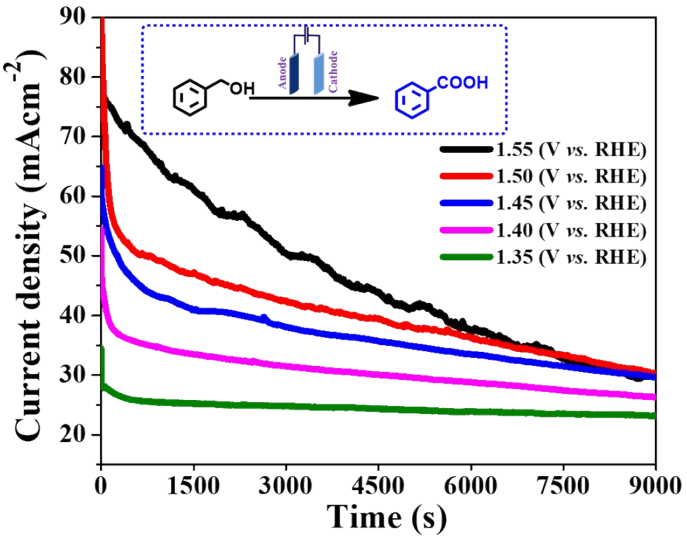

Figure S20. Chronoamperometry study at different potentials for 2.5 h to optimise BOR with CoOOH-1.

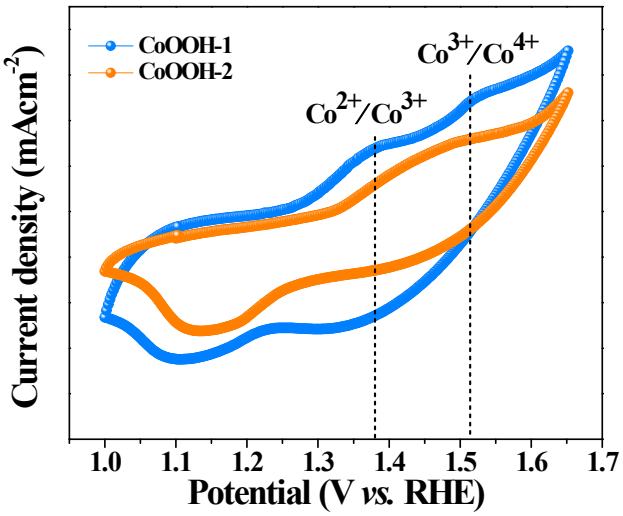

Figure S21. CV profiles of CoOOH-1 and CoOOH-2 showing the redox couple of Co^{2+}/Co^{3+} and Co^{3+}/Co^{4+}.[3–5]

Table S2. Comparison of the BOR activity of CoOOH-1 with literature-reported catalysts.

Catalyst	**Potential (V *vs.* RHE)**	**Current density (mA cm^{-2})**	**FE (%)**	**Reference**
CoOOH-1	**1.53**	**400**	**99**	**This work**
MnFeCoNiCu-PBA	1.57	100	98.9	6
Au/Co(O)OH/NF	1.50	540	99	7
Fe-Co(O)OH	1.47	400	98.3	2
$ZnCo_2O_4$@$Ni(OH)_2$	1.48	100	96	8
$Co(Cu)_{0.5}O_xH_y$	1.50	10	94.95	9
Co-Ni-LDH/NF	1.60	120	87	10
$CoFeO_x$	1.42	50	95	11
hp-Ni/NF	1.42	10	98	12
$Co_{0.83}Ni_{0.17}$/AC	1.42	10	96	13
Co/$Ni(OH)_2$/NF	1.33	100	96	14
Co_3O_4	1.50	86	91.4	15
NiCo-21-MOF	1.52	338.16	-	16
NC@$CuCo_2N_x$	1.25	10	81.3	17
NiO/Ni_3S_2	1.609	50	94	18
ZnO/Co_3O_4@$Ni(OH)_2$/NF	1.46	100	97	19
Ni_2P	1.30	10	95.3	20
$NiCo_2O_4$	1.46	100	99	21
ZIF-9@GO	1.60	204	88	22
CoNi-A	1.38	400	97	23
NiCo-hydroxide	1.35	100	95	24
Ni@Ni/NiO_x	1.309	10	96	25

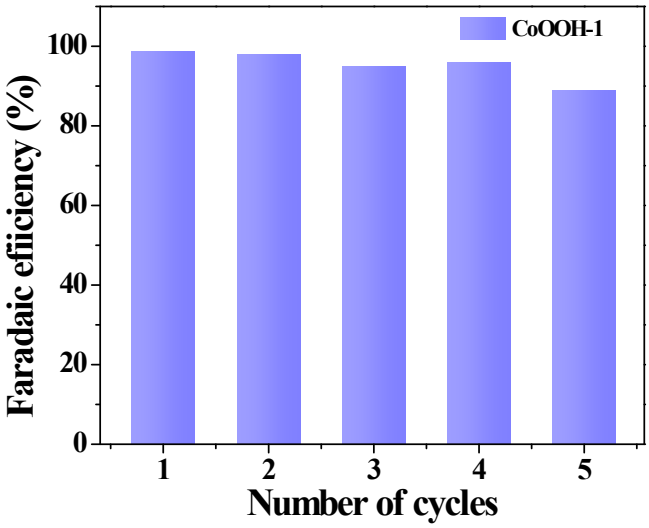

Figure S22. Recycling test of CoOOH-1 for BOR showed excellent stability with minimum activity loss.

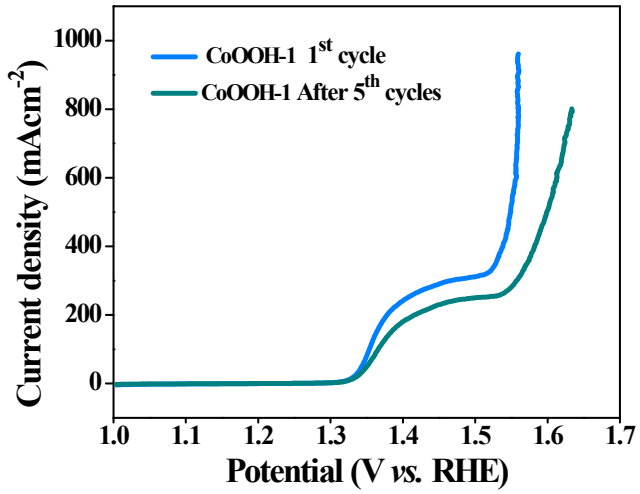

Figure S23. LSV profiles for BOR with CoOOH-1 in the 1st cycle and after 5th cycle.

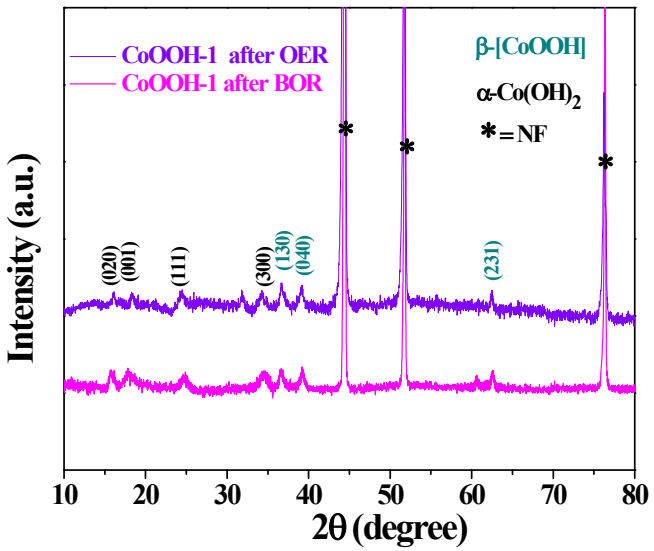

Figure S24. PXRD of CoOOH-1 after 2.5 h of BOR shows no change in the active β-Co(O)OH (JCPDF 26-0480) and α-$Co(OH)_2$ (JCPDF 48-0083) phases, confirming the structural stability of the catalyst.

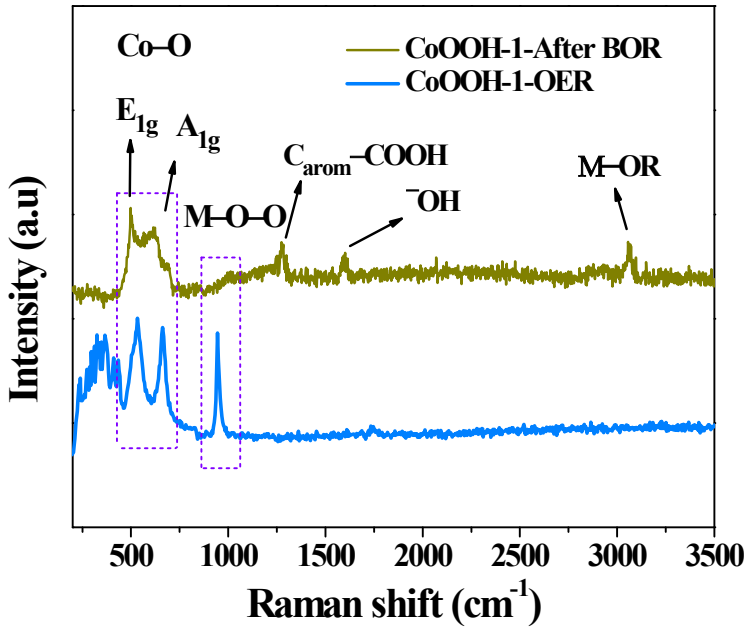

Figure S25. Comparison of Raman spectra of CoOOH-1 after OER (CoOOH-1-OER) and after BOR (CoOOH-1-BOR).

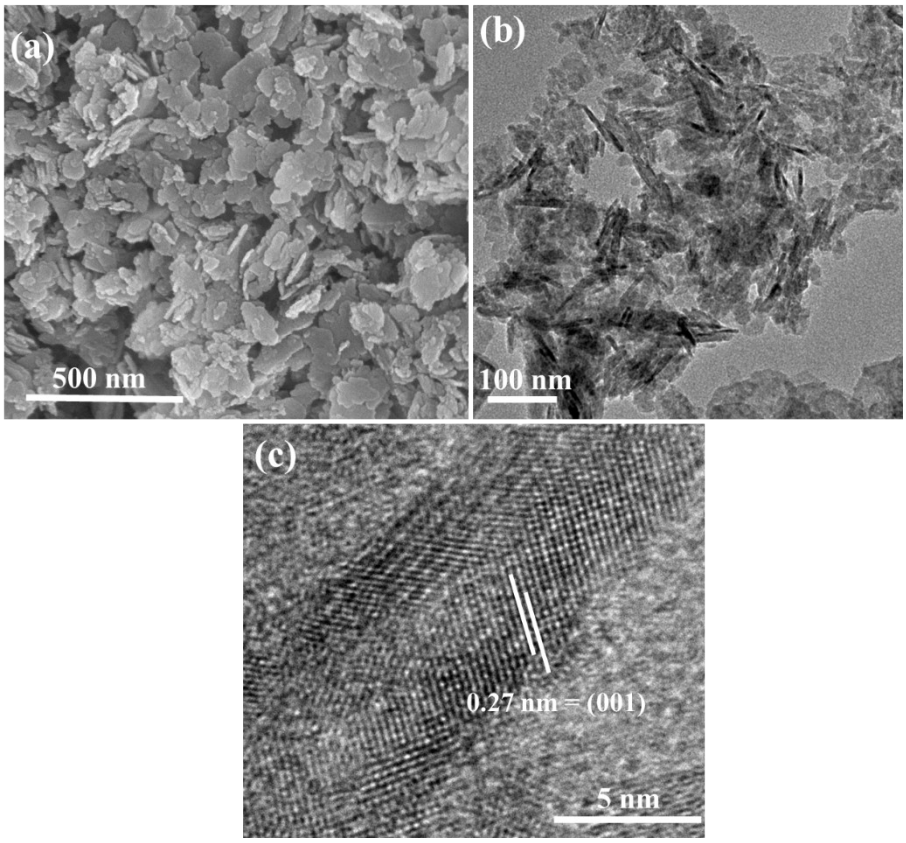

Figure S26. (a) SEM image of CoOOH-1 after BOR. (b) TEM image of CoOOH-1 after BOR. (c) HR-TEM image of CoOOH-1 after BOR, showing the lattice spacing of 0.27 nm, corresponding to the (001) plane of β-CoOOH.

Table S3. Characterisation of the products by ^{1}H NMR and ^{13}C NMR. *It should be noted that, in certain cases, the ^{1}H NMR resonance of the –COOH proton is not detected, likely due to proton exchange or broadening effects.

Benzoic acid 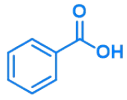	^{1}H NMR (500 MHz, $CDCl_3$) δ: 12.19 (s, 1H), 8.18 (d, *J* = 7.2 Hz, 2H), 7.65 (t, *J* = 7.4 Hz, 1H), 7.52 (d, *J* = 7.7 Hz, 2H). ^{13}C NMR (125 MHz, $CDCl_3$) δ: 172.69, 133.88, 130.27, 129.40, 128.53. **Yield: 99%**
4-trifluromethylbenzoic acid 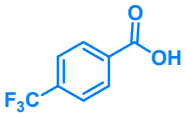	^{1}H NMR (500 MHz, d_6-DMSO) δ: 8.00 (d, 2H), 7.69 (d, 2H). ^{13}C NMR (125 MHz, d_6-DMSO) δ: 166.93, 134.72, 133.18, 132.92, 130.43, 125.87. **Yield: 99%**
4-Cyanobenzoic acid 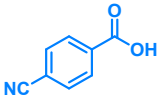	^{1}H NMR (500 MHz, d_6-DMSO) δ: 8.07 (d, *J* = 8.3 Hz, 2H), 7.95 (d, *J* = 8.2 Hz, 2H). ^{13}C NMR (125 MHz, d_6-DMSO) δ: 166.56, 135.28, 133.10, 130.39, 118.65, 115.50. **Yield: 99%**
4-Chlorobenzoic acid 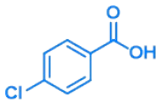	^{1}H NMR (500 MHz, d_6-DMSO) δ: 13.17 (s, 1H), 7.94 (d, *J* = 7.0 Hz, 2H), 7.56 (d, *J* = 12.8 Hz, 2H). ^{13}C NMR (125 MHz, d_6-DMSO) δ: 166.92, 138.26, 131.60, 130.11, 129.17. **Yield: 98%**
2-Chlorobenzoic acid 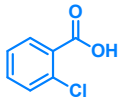	^{1}H NMR (500 MHz, $CDCl_3$) δ: 8.06 (d, *J* = 7.2 Hz, 1H), 7.53 – 7.48 (m, 2H), 7.39 (t, *J* = 6.0 Hz, 1H). ^{13}C NMR (125 MHz, $CDCl_3$) δ: 170.93, 134.79, 133.65, 132.53, 131.55, 128.42, 126.75. **Yield: 90%**
2,5-Dichlorobenzoic acid 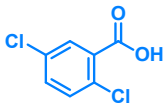	^{1}H NMR (500 MHz, $CDCl_3$) δ: 8.02 (d, *J* = 2.2 Hz, 1H), 7.50 – 7.44 (m, 2H). ^{13}C NMR (125 MHz, $CDCl_3$) δ: 169.25, 133.56, 133.13, 132.80, 132.69, 132.27, 129.63. **Yield: 92%**
2,4,6-Trichlorobenzoic acid 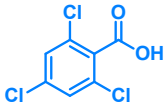	^{1}H NMR (500 MHz, $CDCl_3$) δ: 7.42 (s, 2H). ^{13}C NMR (125 MHz, $CDCl_3$) δ: 168.80, 136.70, 132.61, 131.13, 128.23. **Yield: 99%**
4-Bromobenzoic acid 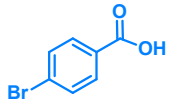	^{1}H NMR (500 MHz, d_6-DMSO) δ: 7.83 (d, *J* = 8.5 Hz, 2H), 7.65 (d, *J* = 8.6 Hz, 2H). ^{13}C NMR (125 MHz, d_6-DMSO) δ: 167.43, 132.15, 131.73, 130.14, 127.51. **Yield: 91%**
4-Methoxybenzoic acid 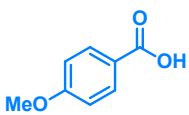	^{1}H NMR (500 MHz, d_6-DMSO) δ: 8.10 (d, *J* = 8.9 Hz, 2H), 6.97 (d, *J* = 8.9 Hz, 2H), 3.90 (s, 3H). ^{13}C NMR (125 MHz, d_6-DMSO) δ: 171.62, 163.89, 132.46, 121.63, 113.69, 55.56. **Yield: 90%**

2,4-Dimethoxybenzoic acid 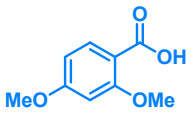	^{1}H NMR (500 MHz, $CDCl_3$) δ: 11.87 (s, 1H), 7.81 (d, 1H), 7.62 (s, 1H), 6.93 (d, 1H), 3.97 (s, *J* = 3.7 Hz, 6H). ^{13}C NMR (125 MHz, $CDCl_3$) δ: 172.08, 153.77, 148.71, 124.62, 121.73, 112.35, 110.35, 56.02. **Yield: 91%**
2,4,6-Trimethoxybenzoic acid 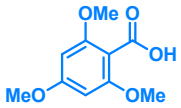	^{1}H NMR (500 MHz, $CDCl_3$) δ: 12.20 (s, 1H), 7.40 (s, 2H), 3.95 (s, 9H). ^{13}C NMR (125 MHz, $CDCl_3$) δ: 171.84, 153.00, 143.06, 124.10, 107.47, 60.96, 56.27. **Yield: 90%**
4-Tert-butylbenzoic acid 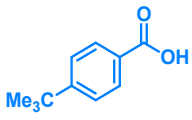	^{1}H NMR (500 MHz, $CDCl_3$) δ: 12.59 (s, 1H), 8.09 (s, 2H), 7.53 (s, 2H), 1.39 (s, 9H). ^{13}C NMR (125 MHz, $CDCl_3$) δ: 172.60, 157.62, 130.15, 126.61, 125.50, 35.21, 31.11. **Yield: 88%**

^{1}H and ^{13}C NMR spectra of the products.

^{1}H and ^{13}C NMR spectra of benzoic acid

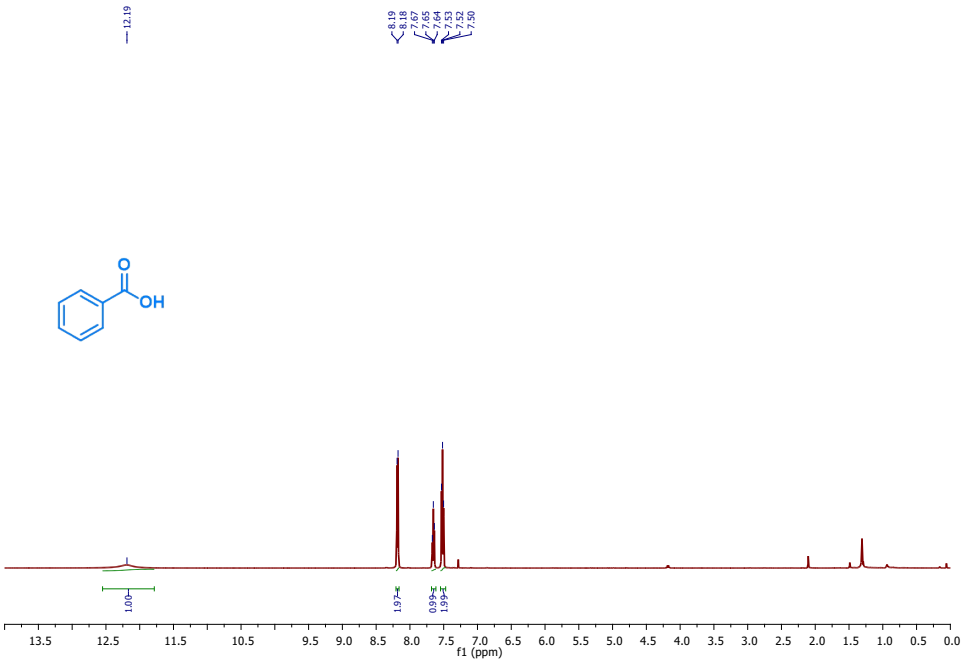

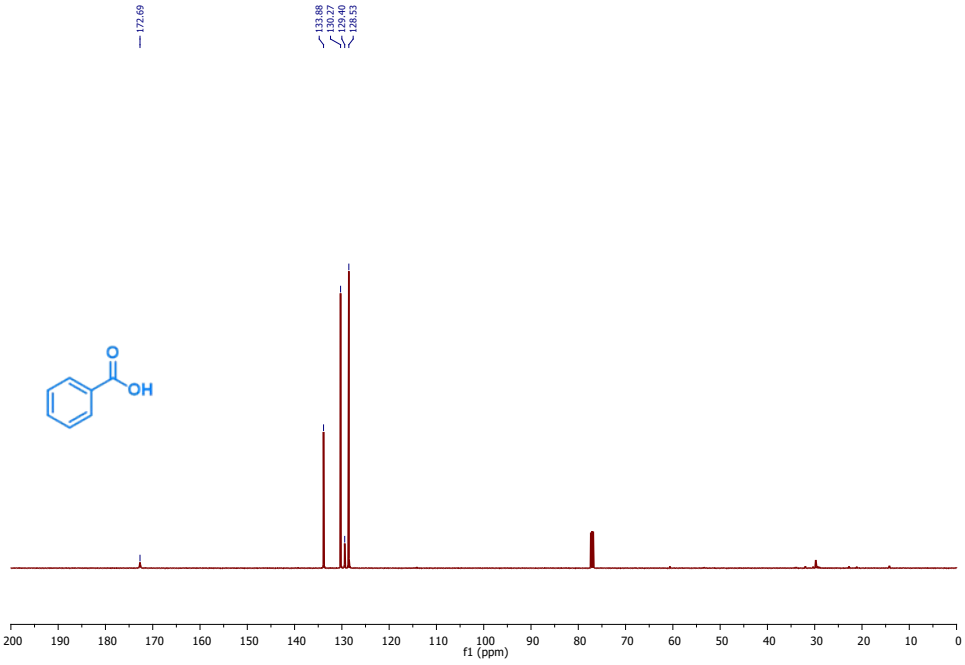

^{1}H and ^{13}C NMR spectra of 4-trifluromethylbenzoic acid

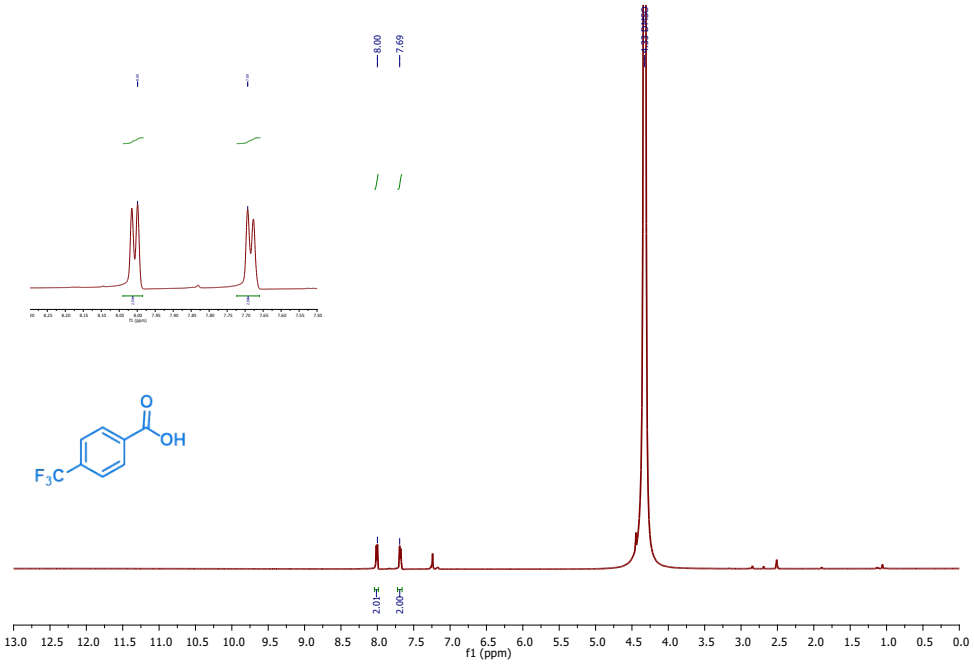

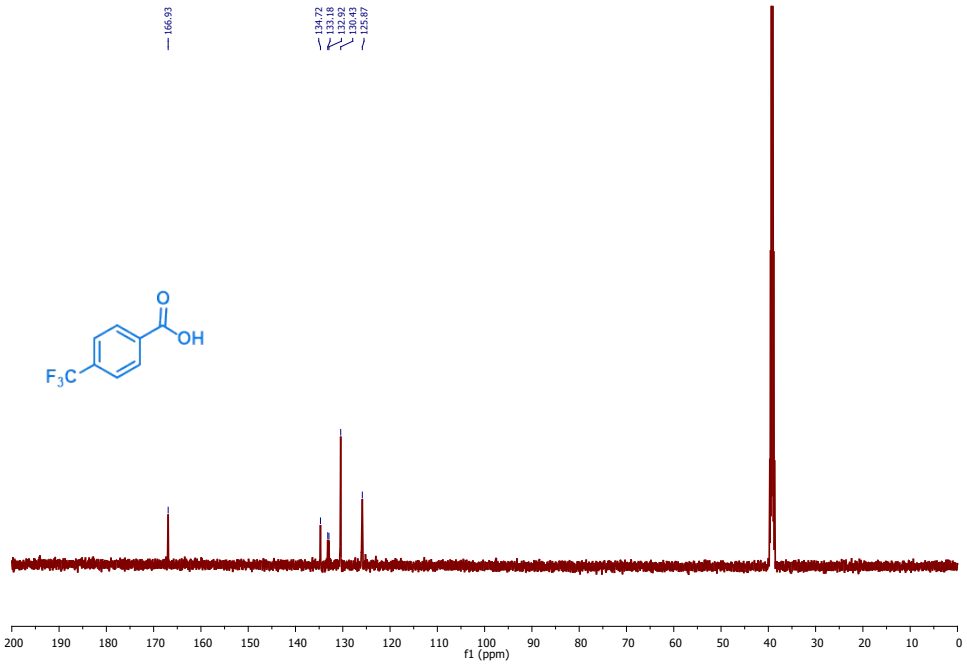

^{1}H and ^{13}C NMR spectra of 4-Cyanobenzoic acid

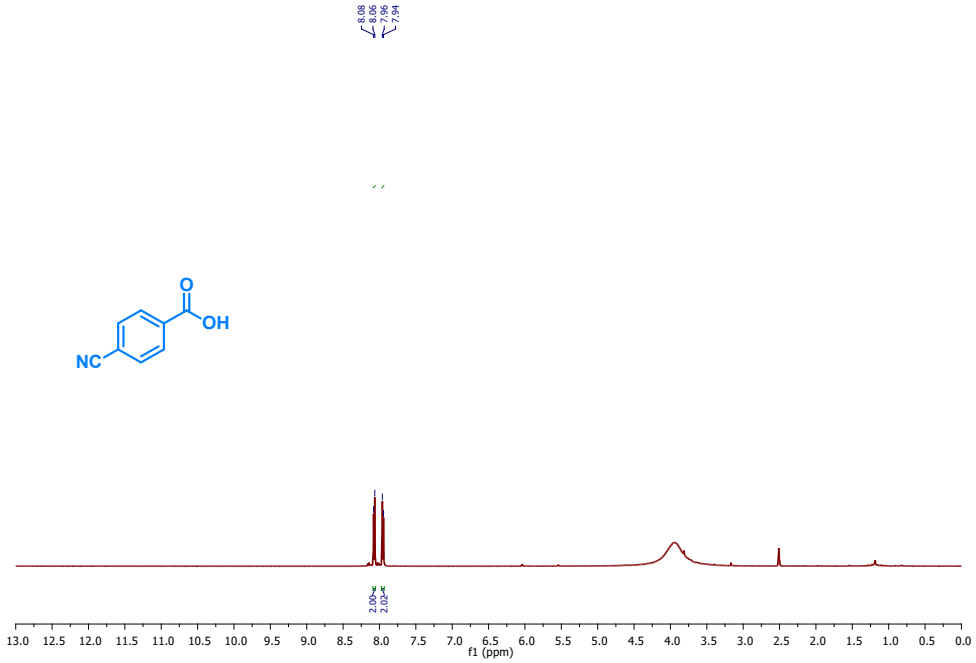

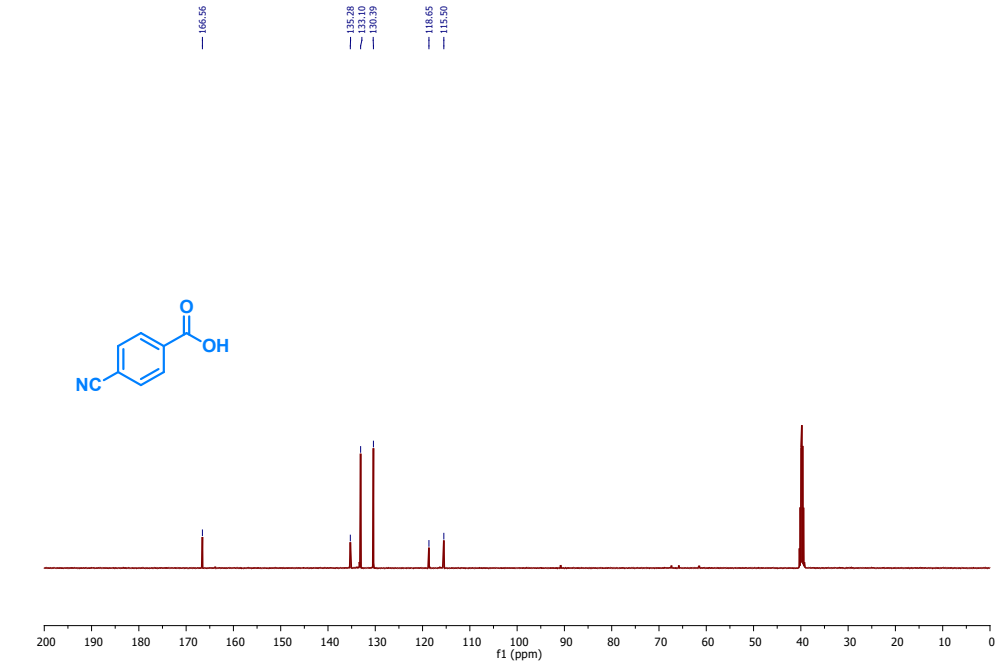

^{1}H and ^{13}C NMR spectra of 4-Chlorobenzoic acid

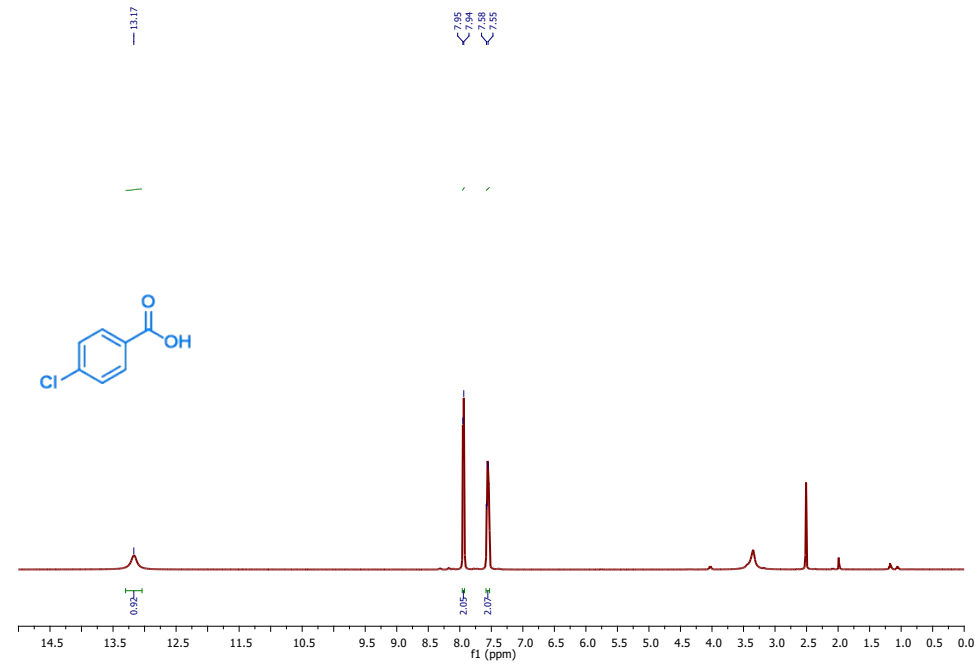

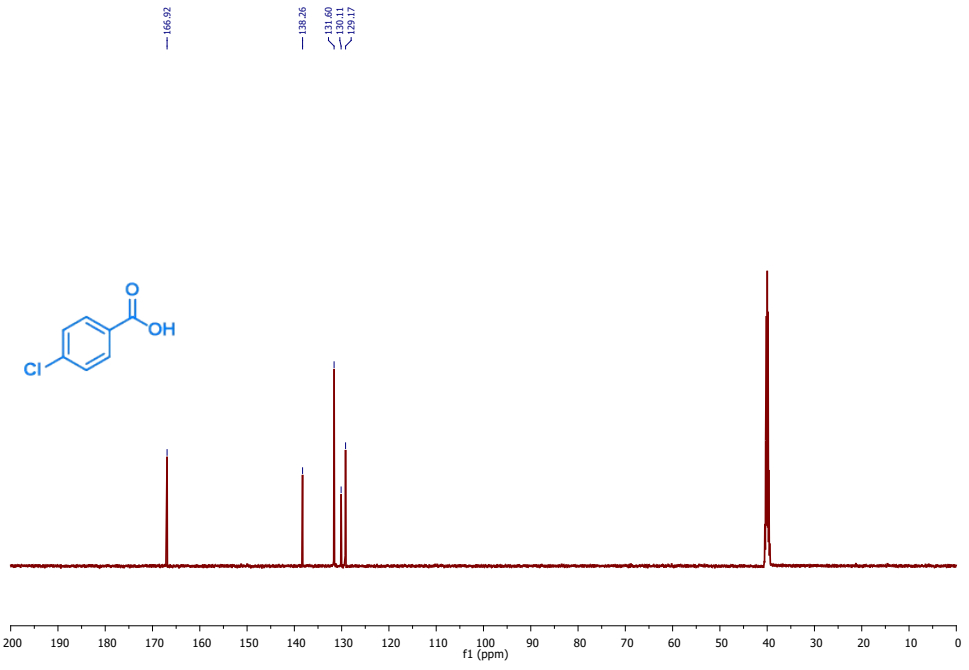

^{1}H and ^{13}C NMR spectra of 2-Chlorobenzoic acid

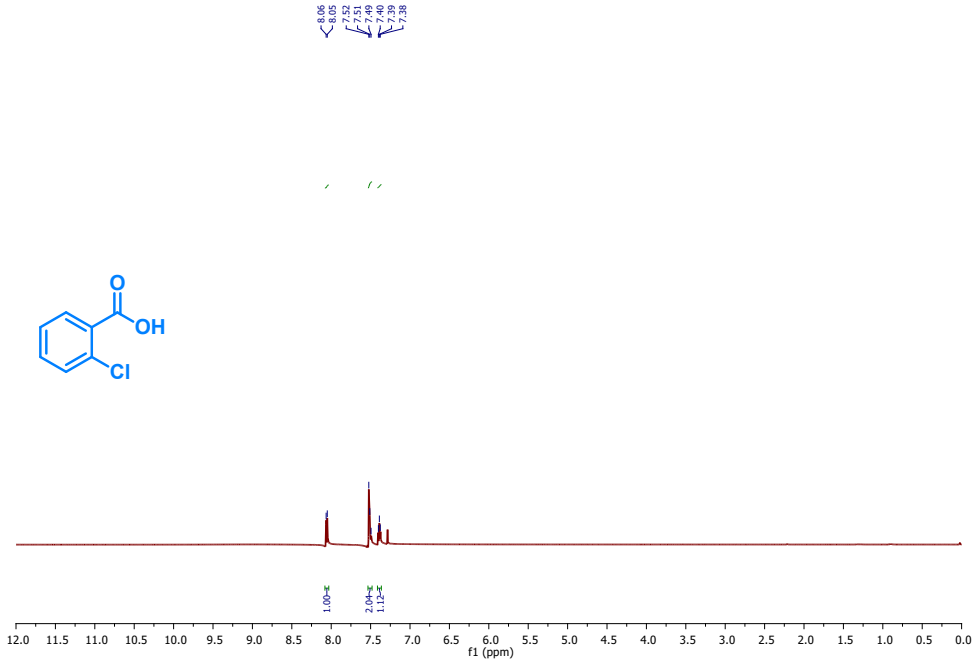

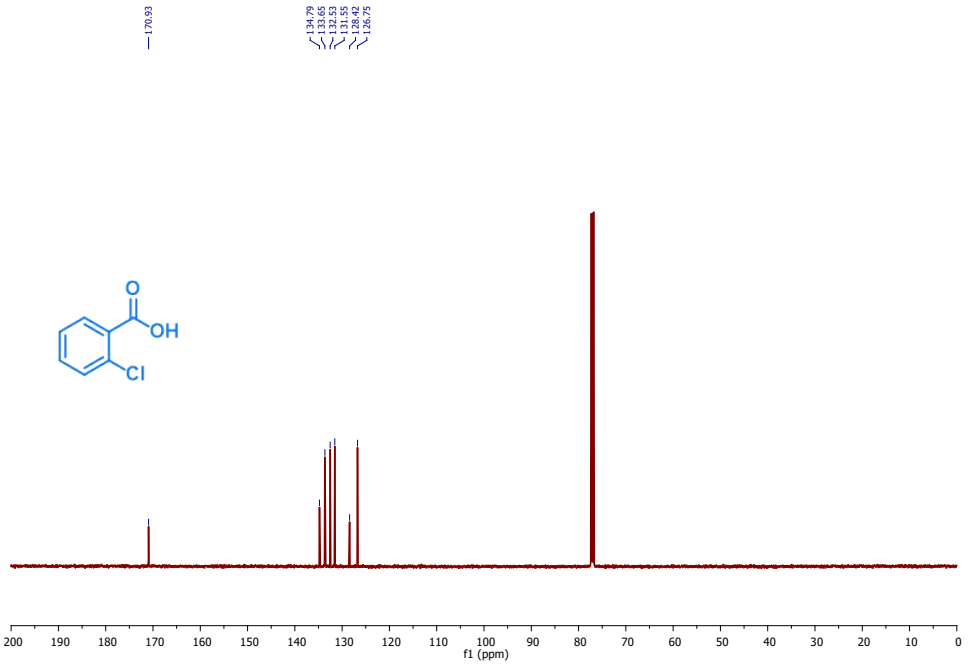

^{1}H and ^{13}C NMR spectra of 2,5-Dichlorobenzoic acid

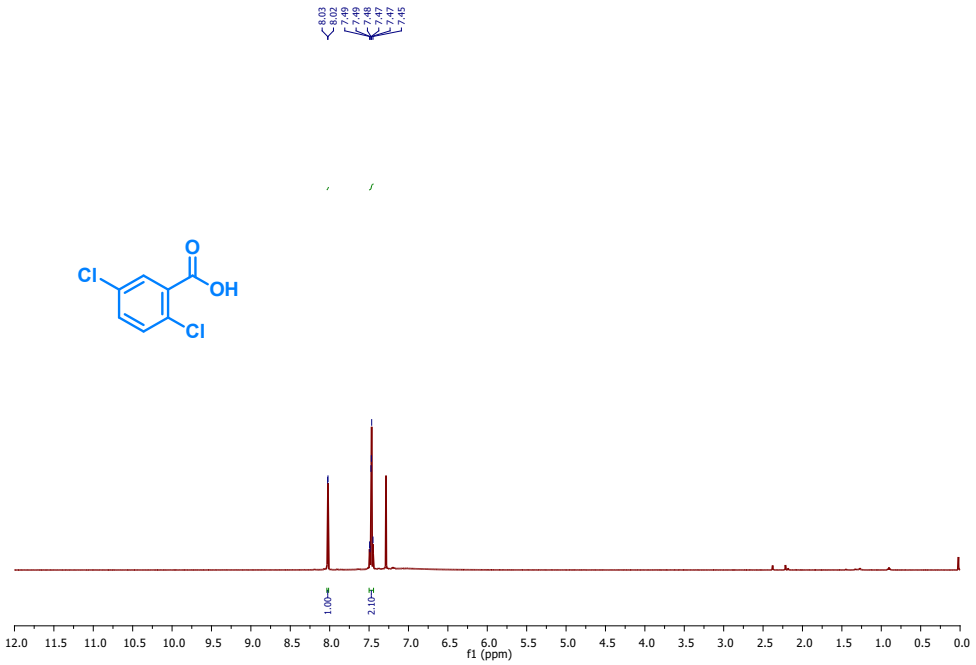

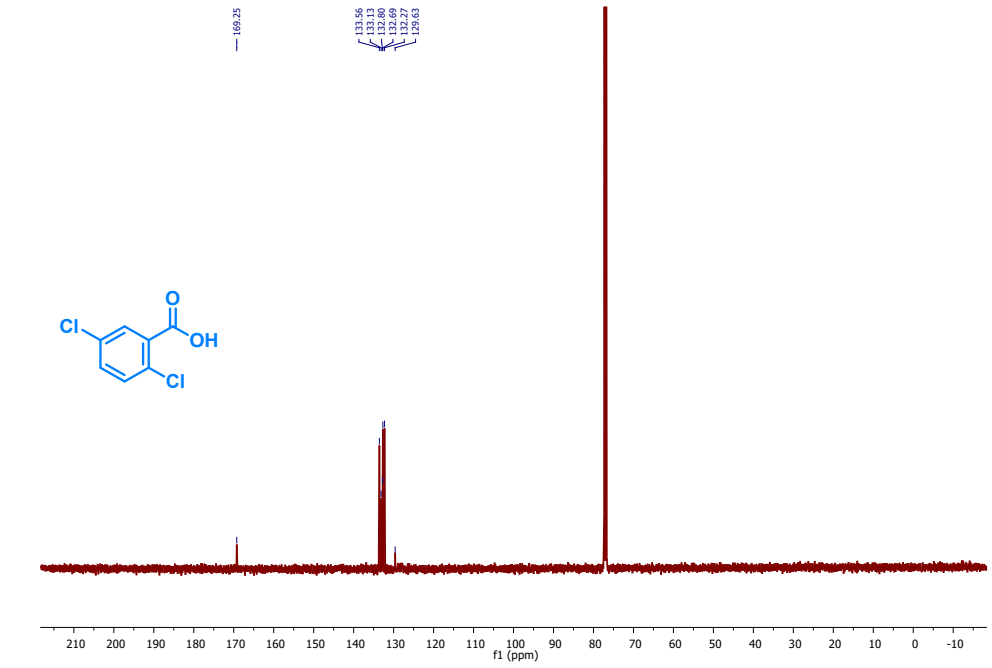

^{1}H and ^{13}C NMR spectra of 2,4,6-Trichlorobenzoic acid

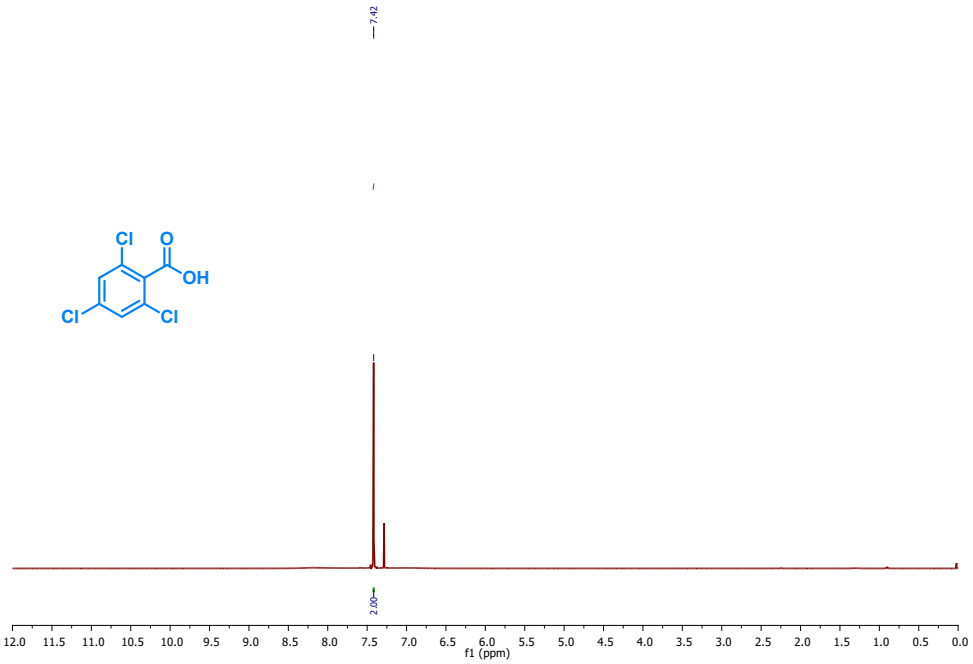

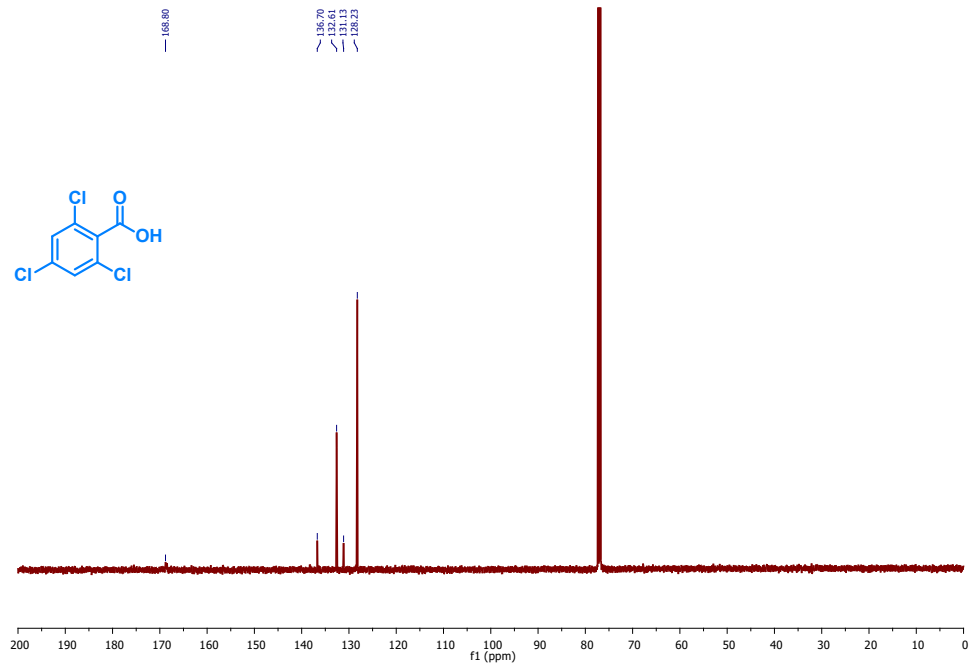

^{1}H and ^{13}C NMR spectra of 4-Bromobenzoic acid

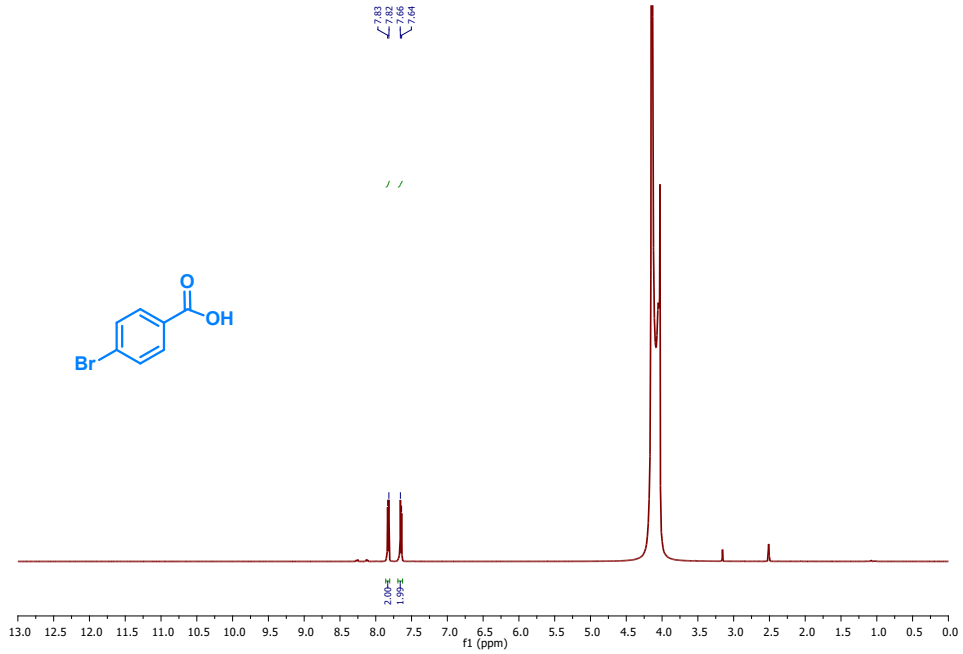

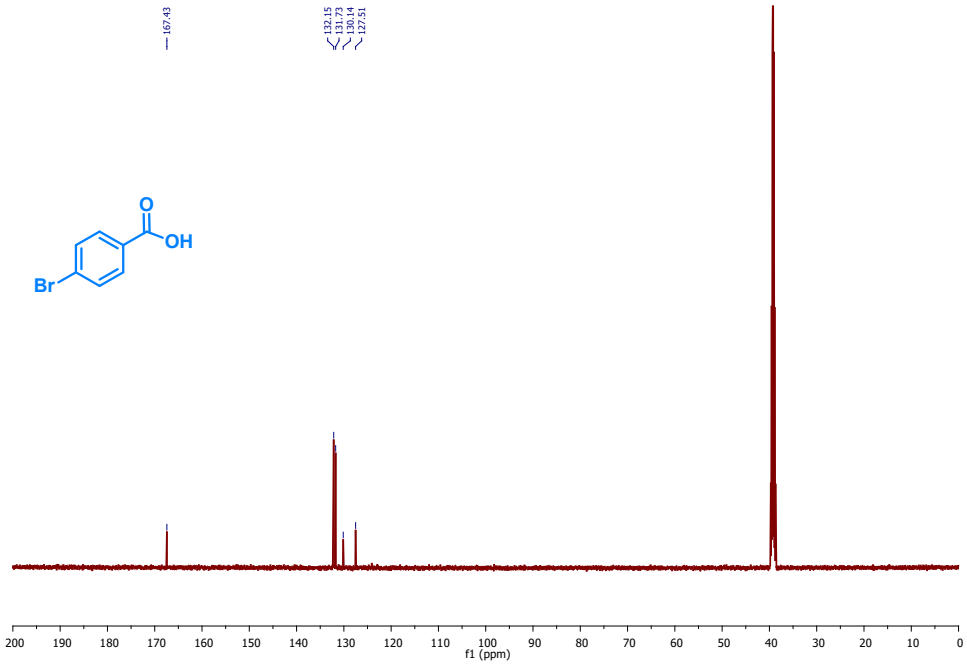

^{1}H and ^{13}C NMR spectra of 4-Methoxybenzoic acid

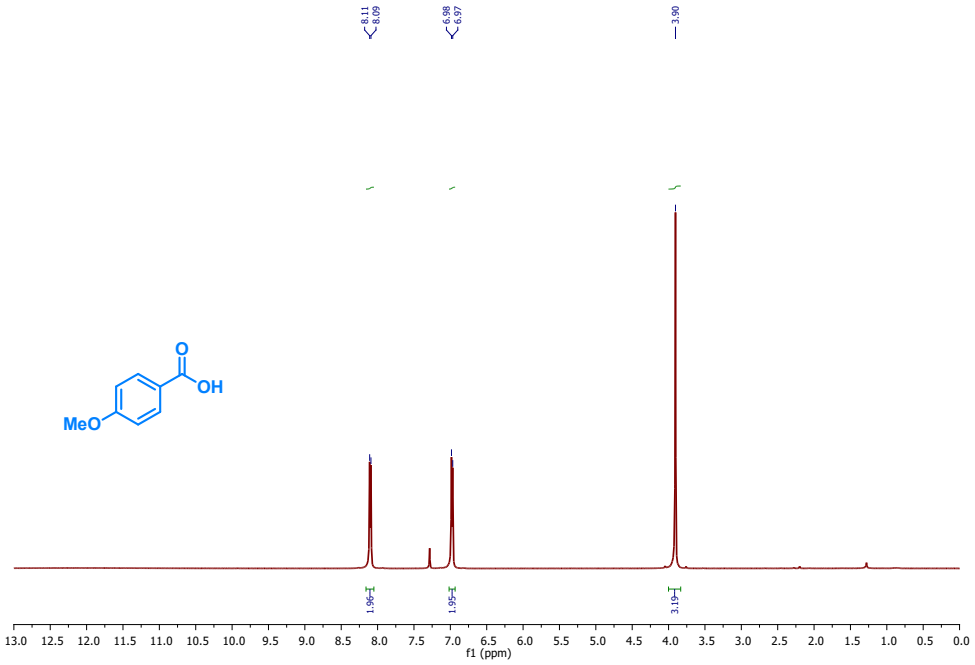

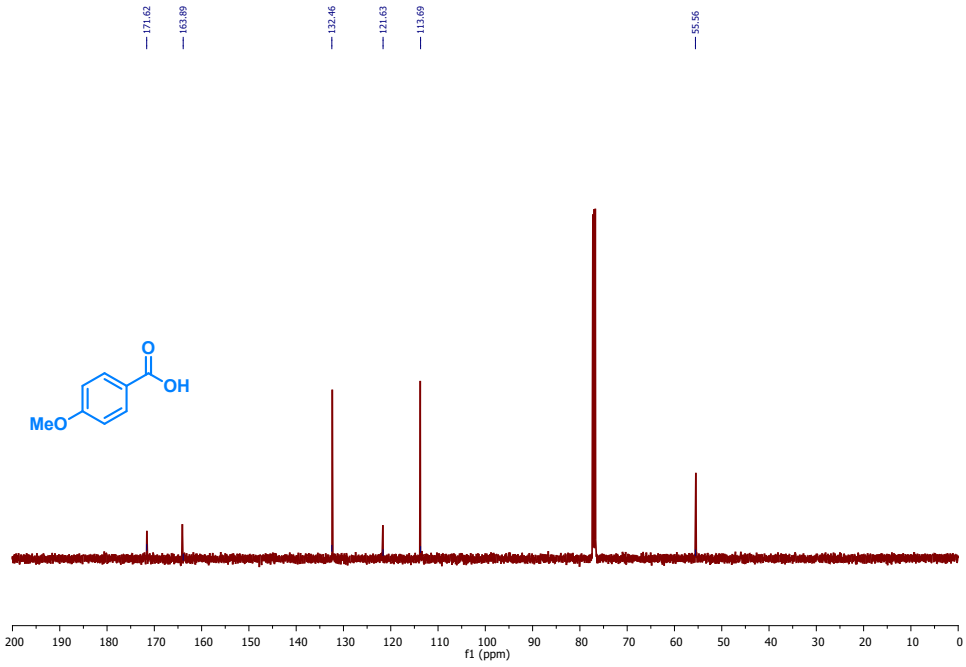

^{1}H and ^{13}C NMR spectra of 2,4-Dimethoxybenzoic acid

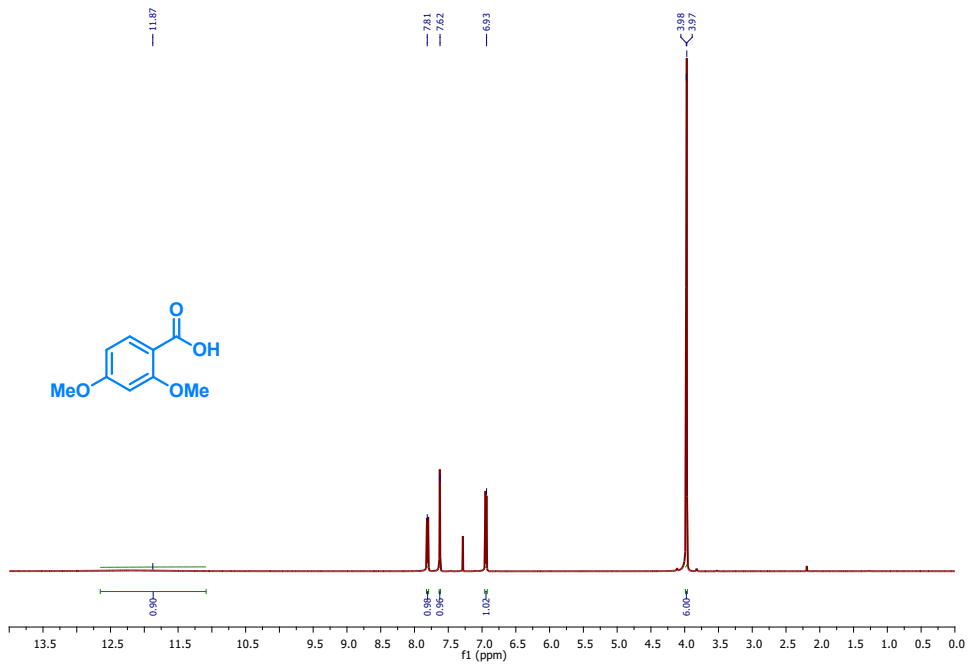

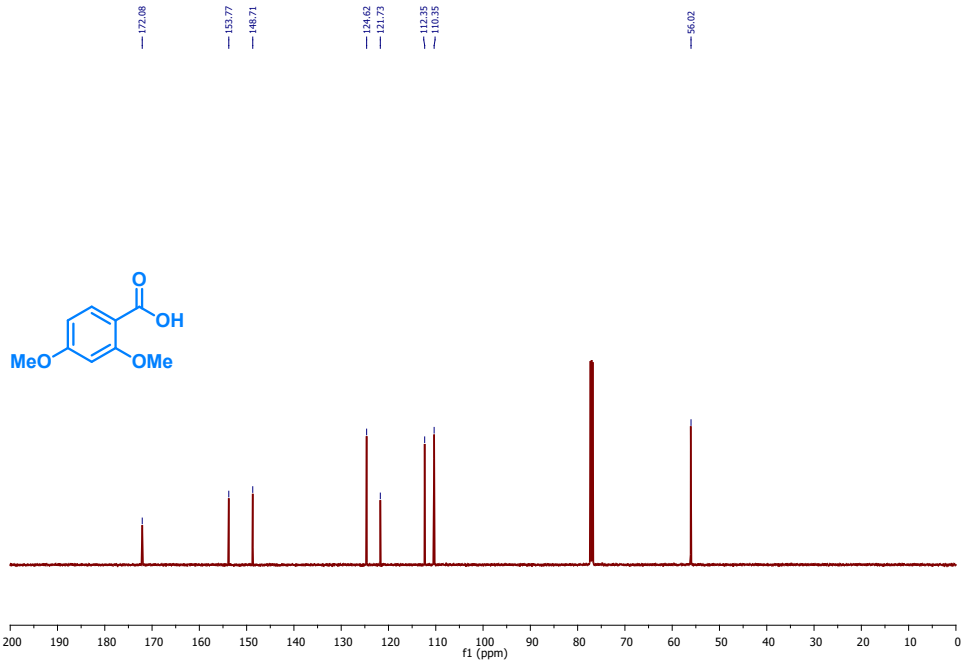

^{1}H and ^{13}C NMR spectra of 2,4,6-Trimethoxybenzoic acid

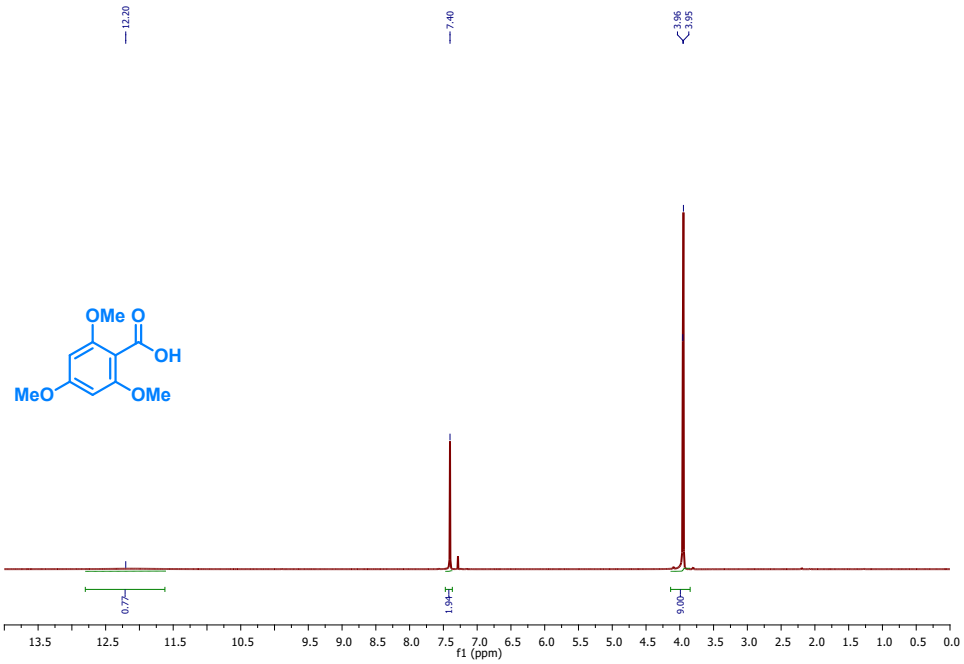

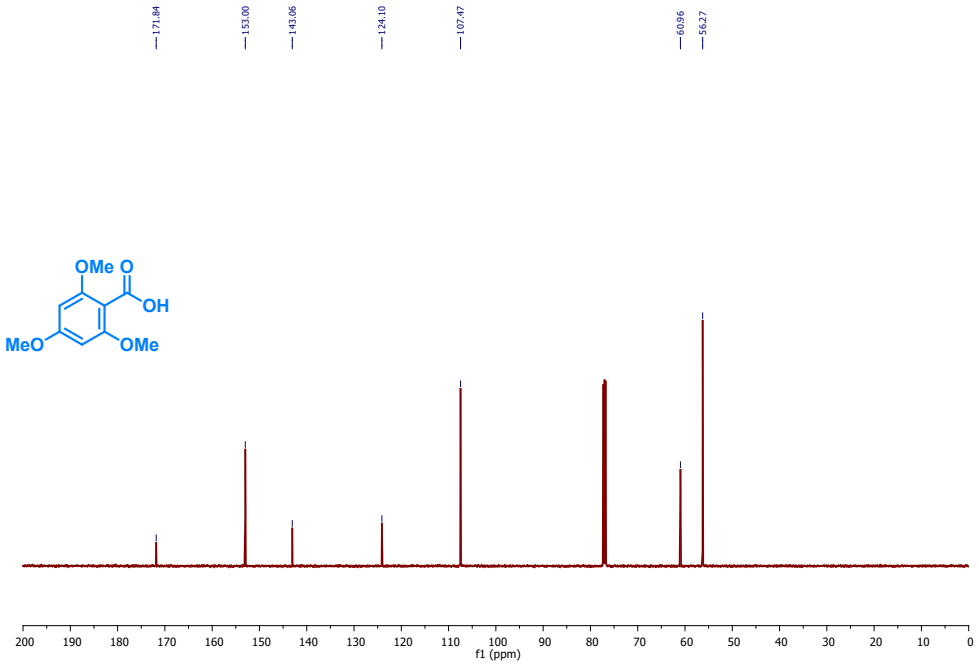

^{1}H and ^{13}C NMR spectra of 4-tert-butylbenzoic acid

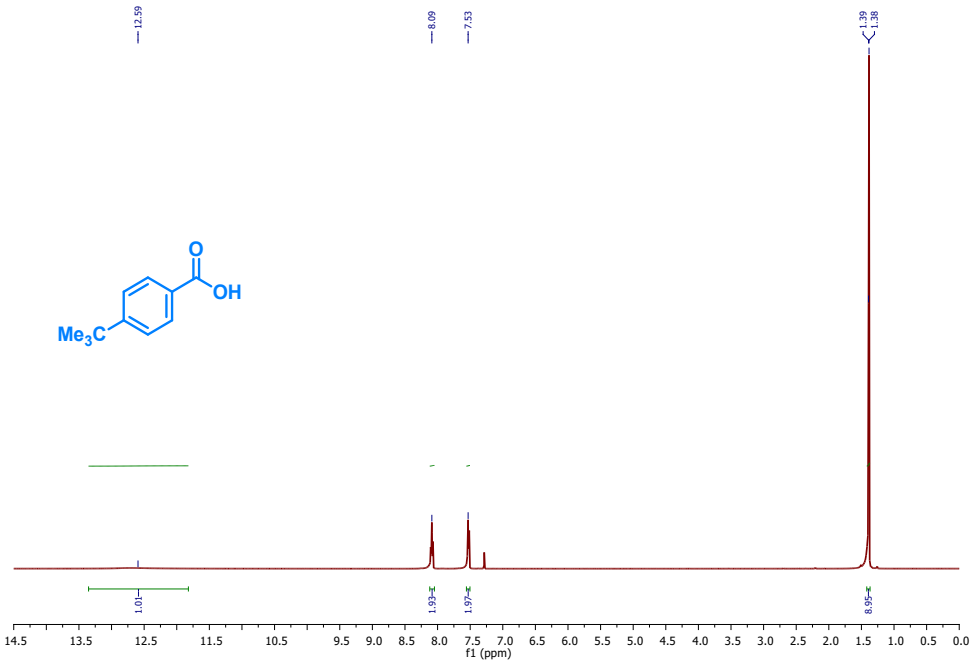

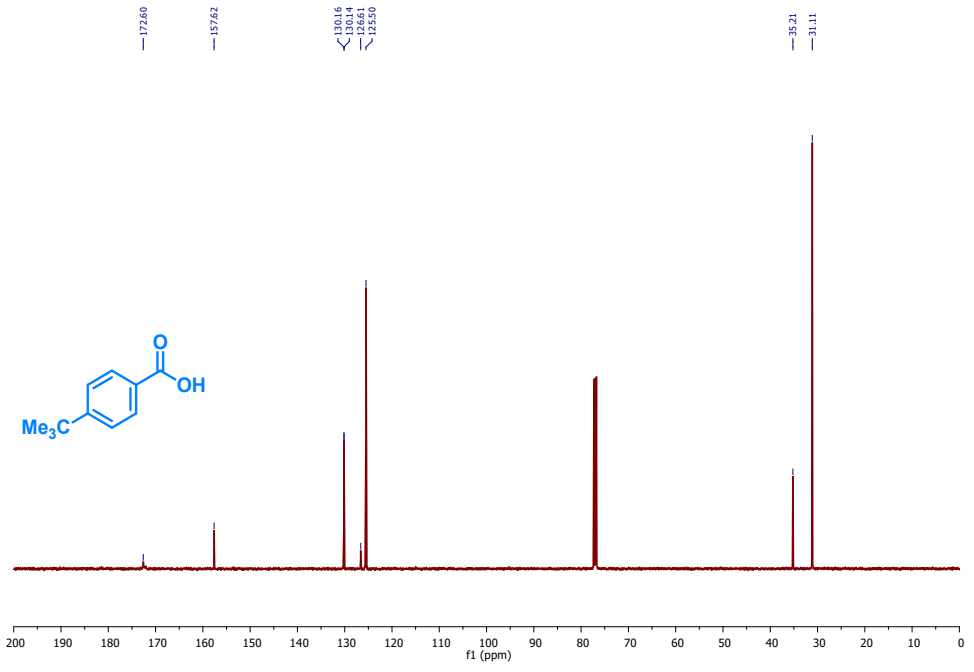

References

1 H. Zou, X. Liu, K. Wang, Y. Duan, C. Wang, B. Zhang, K. Zhou, D. Yu, L. Y. Gan and X. Zhou, *Chem. Commun.*, 2021, **57**, 8011–8014.

2 B. Singh, T. Ansari, N. Verma, Y. C. Huang, P. Mannu, C. L. Dong and A. Indra, *J. Mater. Chem. A*, 2024, **12**, 19321–19330.

3 J. Dong, D. W. Boukhvalov, C. Lv, M. G. Humphrey, C. Zhang and Z. Huang, *J. Mater. Chem. A*, 2023,

11, 16683–16694.

4 N. Li, R. G. Hadt, D. Hayes, L. X. Chen and D. G. Nocera, *Nat. Commun.*, 2021, **12**, 4218.

5 W. H. Antink, S. Lee, S. Lee, H. Shin, T.Y. Yoo, W. Ko, J. Shim, G. Na, Y.E. Sung and T. Hyeon, *Adv. Funct. Mater.* 2024, **34**, 2309438.

6 B. Singh, N. Verma, P. Arora and A. Draksharapu, *ACS Appl. Nano Mater.*, 2024, **7**, 27064–27070.

7 Z. Li, Y. Yan, S. M. Xu, H. Zhou, M. Xu, L. Ma, M. Shao, X. Kong, B. Wang, L. Zheng and H. Duan, *Nat. Commun.*, 2022, **13**, 147.

8 J. K. Li, A. Wang, X. Y. Dong, S. Huang, Y. Meng and J. L. Song, *Int. J. Hydrogen Energy*, 2024, **49**, 228–237.

9 L. Huang, X. Lin, K. Zhang, J. Zhang, C. Wang, S. Qu and Y. Wang, *Appl. Catal. B Environ.*, 2024, **346**, 123739.

10 N. Shilpa, A. Pandikassala, P. Krishnaraj, P. S. Walko, R. N. Devi and S. Kurungot, *ACS Appl. Mater. Interfaces*, 2022, **14**, 16222–16232.

11 Y. Huang, R. Yang, G. Anandhababu, J. Xie, J. Lv, X. Zhao, X. Wang, M. Wu, Q. Li and Y. Wang, *ACS Energy Lett.*, 2018, **3**, 1854–1860.

12 B. You, X. Liu, X. Liu and Y. Sun, *ACS Catal.*, 2017, **7**, 4564–4570.

13 G. Liu, X. Zhang, C. Zhao, Q. Xiong, W. Gong, G. Wang, Y. Zhang, H. Zhang and H. Zhao, *New J. Chem.*, 2018, **42**, 6381–6388.

14 L. Ming, X. Y. Wu, S. S. Wang, W. Wu and C. Z. Lu, *Green Chem.*, 2021, **23**, 7825–7830.

15 Y. Cao, D. Zhang, X. Kong, F. Zhang and X. Lei, *J. Mater. Sci.*, 2021, **56**, 6689–6703.

16 G. Sun, W. Zhang, Y. Song, M. Yuan, W. Su, D. Guo and X. Chen, *Inorg. Chem.*, 2022, **61**, 7308–7317.

17 J. Zheng, X. Chen, X. Zhong, S. Li, T. Liu, G. Zhuang, X. Li, S. Deng, D. Mei and J. G. Wang, *Adv. Funct. Mater.*, 2017, **27**, 1–11.

18 R. Li, P. Kuang, L. Wang, H. Tang and J. Yu, *Chem. Eng. J.*, 2022, **431**, 134137.

19 J. K. Li, A. Wang, X. Y. Dong, S. Huang, Y. Meng and J. L. Song, *New J. Chem.*, 2023, **47**, 5970–5976.

20 F. Li, C. Liu, H. Lin, Y. Sun, H. Yu, S. Xue, J. Cao, X. Jia and S. Chen, *J. Colloid Interface Sci.*, 2023, **640**, 329–337.

21 M. Xu, J. Geng, H. Xu, S. Zhang and H. Zhang, *Inorg. Chem. Front.*, 2023, **10**, 2053–2059.

22 S. Chongdar, A. Ghosh, R. Bal and A. Bhaumik, *J. Mater. Chem. A*, 2023, **12**, 233–246.

23 T. Ansari, D. Bagchi, S. Ghosh, J. Niklas Hausmann, A. Indra and P. W. Menezes, *Chem. - A Eur. J.*, 2025, **31**, 1–8.

24 H. Huang, C. Yu, X. Han, H. Huang, Q. Wei, W. Guo, Z. Wang and J. Qiu, *Energy Environ. Sci.*, 2020, **13**, 4990–4999.

25 R. Li, P. Kuang, S. Wageh, A. A. Al-Ghamdi, H. Tang and J. Yu, *Chem. Eng. J.*, 2023, **453**, 139797.